ADVANCED FUNCTIONAL MATERIALS
www.afm-journal.de

Two-Dimensional Molybdenum Trioxide and Dichalcogenides

Sivacarendran Balendhran, Sumeet Walia, Hussein Nili, Jian Zhen Ou, Serge Zhuiykov, Richard B. Kaner, Sharath Sriram, Madhu Bhaskaran, and Kourosh Kalantar-zadeh**

In the quest to discover the properties of planar semiconductors, two-dimensional molybdenum trioxide and dichalcogenides have recently attracted a large amount of interest. This family, which includes molybdenum trioxide (MoO_3), disulphide (MoS_2), diselenide ($MoSe_2$) and ditelluride ($MoTe_2$), possesses many unique properties that make its compounds appealing for a wide range of applications. These properties can be thickness dependent and may be manipulated via a large number of physical and chemical processes. In this Feature Article, a comprehensive review is delivered of the fundamental properties, synthesis techniques and applications of layered and planar MoO_3, MoS_2, $MoSe_2$, and $MoTe_2$ along with their future prospects.

1. Introduction

Very soon after the discovery of graphene, other two dimensional (2D) materials, such as metal chalcogenides and transition metal oxides, regained research interest.[1] So far amongst 2D materials, molybdenum compounds have played a significant role. Molybdenum trioxide and dichalcogenides (MT&Ds) have shown intriguing physical and chemical properties as well as exciting prospects for a variety of applications. Similar to graphite, MT&Ds are found in layered forms that can be exfoliated into small thicknesses containing mono- or multiple-layers.[2–5] In the past decade, the interest in such materials, in particular molybdenum disulfide (MoS_2), has increased exponentially due to their potential uses as 2D semiconducting materials with remarkable electronic and optical properties, which can be thickness dependent and easily engineered.[5–7]

Traditionally, MT&Ds have been largely used in lubrication and electrochemical products. However, the new discoveries regarding their low dimensional electronic structures have led to possibilities for their incorporation into many other exciting applications. Bandgap energy of mono- or multi-layered MT&Ds can be manipulated using chemical processes such as ionic intercalation or physical processes such as applying stress or electric fields.[8–10] Remarkably, molybdenum dichalcogenide's (MDs) electronic structure is layer dependent and shows a natural transition from indirect to direct bandgap,[6,7] and molybdenum trioxide (MT) transform from semiconducting to metallic by careful intercalation of ionic components.[11]

MT&Ds are relatively abundant in nature, their deposition is compatible with standard microfabrication techniques and layered MT&Ds are generally considered stable and non-hazardous. There are a variety of techniques for the synthesis of 2D MT&Ds, many of them have been adopted from their bulk counterparts and many other layer specific synthesis methods have been recently developed.

The layered MT&Ds have already shown significant applications in various fields of optics, electrochemistry, electronics and sensors. There have been recent important advancements in the development of 2D field effect transistors with relatively high electron mobilities based on both molybdenum trioxide (MoO_3) and MoS_2.[2,5] There have also been demonstrations of many applications based on direct bandgap mono-layered MoS_2 and its strong photoluminescence in optical and sensing systems.[12–14]

The appearance of a large number of reports on one-dimensional (1D) and 2D MDs has created a demand for their comprehensive review. Additionally, 1D and 2D MTs are also rapidly gaining scientific interest. Recent progress in 1D structures of MT&Ds, such as single- and multi-walled nanotubes have been reported elsewhere.[15] Considering that 2D MT and MDs have many common applications, owing to their similar layered nature, in this feature article we present and analyze the progress of research on layered and planar MT&Ds. This article describes the fundamental properties of mono- and multi-layered MT&Ds investigated to date. It discusses different

S. Balendhran, S. Walia, H. Nili, Dr. J. Z. Ou,
Dr. S. Sriram, Dr. M. Bhaskaran, Prof. K. Kalantar-zadeh
School of Electrical and Computer Engineering
RMIT University
Melbourne, Victoria, Australia
E-mail: shiva.balendhran@rmit.edu.au,
sivacarendran.balendhran@csiro.au; kourosh.kalantar@rmit.edu.au
S. Balendhran, Dr. S. Zhuiykov
Materials Science and Engineering Division
CSIRO, Highett, Victoria, Australia
H. Nili, Dr. S. Sriram, Dr. M. Bhaskaran
Functional Materials and Microsystems Research Group
RMIT University
Melbourne, Victoria, Australia
Prof. R. B. Kaner
Department of Chemistry and Biochemistry
University of California
Los Angeles, California, USA

DOI: 10.1002/adfm.201300125

techniques for the manipulation of such properties. This feature article provides a detailed outlook on the common synthetic processes, how to identify both mono- and multi-layered MT&Ds and applications of layered MT&Ds reported thus far.

2. Properties of Mono- and Multi-Layered MoO_3, MoS_2, $MoSe_2$, and $MoTe_2$

In this section, the basic crystal structures of layered MT&Ds are described. The fundamental electronic, optical, and mechanical properties are discussed in detail.

2.1. Crystal Structure

2.1.1. MoO_3

MoO_3 is generally found in two major crystal phases: thermodynamically stable α-MoO_3 and metastable β-MoO_3.[3,16–18] Orthorhombic α-MoO_3 possesses the much desired layered crystal phase of molybdenum trioxide. It consists of dual layer planar crystals of distorted MoO_6 octahedra, held together in the vertical [010] direction by weak van der Waals forces (**Figure 1**a), while the internal bonds in the octahedra are dominated by covalent and ionic bonds.[3,17] Each of the double layers form edge sharing zig-zag rows along the [001] and corner sharing rows along the [100] directions, respectively. Lattice constants of α-MoO_3 (space group *Pbnm*) are a = 3.962 Å, b = 13.855 Å, and c = 3.699 Å.[3,18]. β-MoO_3 adopts a monoclinic 3D structure.[18,19] Unlike α-MoO_3, the MoO_6 octahedra that forms β-MoO_3, shares corners in all three dimensions, establishing a 3D structure that is not desirable for forming planar crystals. The β phase is generally observed to be transformed into the more stable, layered α-MoO_3 phase above 350 °C.[16,17]

2.1.2. MoX_2 -MoS_2, $MoSe_2$ and $MoTe_2$

Monolayers of MoX_2 compounds (X = S, Se, and Te) are typically composed of Mo atoms sandwiched between X atoms, organized in a 2D hexagonal honeycomb structure. The bulk layered material is comprised of vertically stacked monolayers bound together by weak van der Waals forces (Figure 1b). Common polymorphs of MoX_2 compounds are hexagonal 2*H*-MoX_2 and rhombohedral 3*R*-MoX_2 that are different in vertical stacking alignment.[20,21] 2*H*-MoX_2 is composed of monolayers that are vertically stacked in ABAB sequence, while 3*R*-MoX_2 is comprised of ABCABC sequence.[21,22] However, 2*H*-MoX_2 is the naturally occurring and relatively stable polytype observed for MoX_2 compounds, while 3*R*-MoX_2 is generally transformed into the 2*H*-MoX_2 upon heating.[22] Hence, we consider the dominant and stable 2*H*-MoX_2 polytype in this review. The lattice parameters of the layered 2*H*-MoX_2 compounds are presented in **Table 1**.

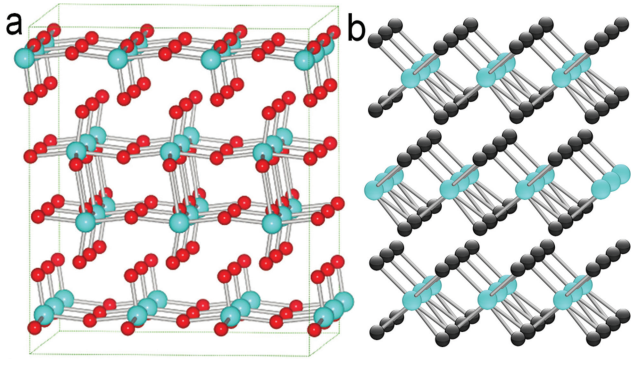

Figure 1. Crystal structure of a) layered α-MoO_3 and b) 2*H*-MoX_2 (blue, red and black spheres represent Mo, O, and chalcogen atoms, respectively). a) Reproduced with permission.[18] Copyright 2010, American Chemical Society.

Sivacarendran Balendhran is in the final stage of his Ph.D candidature at the School of Electrical and Computer Engineering, RMIT University, Australia. Prior to his Ph.D. candidature, he received his Bachelor of Engineering (Electrical Engineering, First Class Honours) from the same university in 2009. Sivacarendran's research interests include two-dimensional semiconductors, nanostructure synthesis and micro/nano fabrication.

Kourosh Kalantar-zadeh is a Professor at RMIT University, Australia. He received his B.Sc. (1993) and M.Sc. (1997) degree from Sharif University of Technology, Iran, and Tehran University, Iran, respectively, and his Ph.D. from RMIT University, Australia (2001). His research interests include chemical and biochemical sensors, nanotechnology, microsystems, materials sciences, electronic circuits, and microfluidics.

2.2. Electronic Structure

2.2.1. Band Structure and Bandgap Tuning

MoO_3: Bulk α-MoO_3 is an indirect wide bandgap material (>3 eV), but offers bandgap tunability via a range of appr oaches.[2,11,23,24] The most common procedure adopted is hydrogen intercalation into the crystal lattice.[2,23] Other alkali metals such as Li, Na, K as well as organic compounds have

Table 1. Properties of 2*H*-MoX_2 compounds.

		MoS_2	$MoSe_2$	$MoTe_2$
Lattice constants [Å][34]	*a*	3.160	3.288	3.517
	c	6.147	6.460	6.981
	c/*a*	1.945	1.962	1.984
Interlayer height [Å]	*X–M*	3.19	3.23	3.63
van der Waals gap [Å]	*X–X*	3.47	3.75	3.92
Bandgap energy [eV][6]	*Bulk*	1.29	1.1	1.0
	Monolayer	1.89	1.58	1.23
Born effective charge[35]	e^*_T	1.1*e*	2.1*e*	3.4*e*
Raman active modes [cm^{-1}][34,35]	A_{1g}	409	243	171
	E^1_{2g}	383	283	232.4
	E_{1g}	287	168.8	116.8
Monolayer relaxed ion elastic coefficients[43]	C_{11}	130	108	80
	C_{12}	32	25	21
Poisson ratio	ν_∞	0.34	0.35	0.37
Monolayer relaxed ion piezoelectric coefficient [pmV^{-1}]	d_{11}	3.73	4.72	9.13
Thermal conductivity [$Wm^{-1}K^{-1}$]	*k*	18.06	2.3	2
Peak Seebeck coefficient [μVK^{-1}][151]	*S*	–580	–900	–780

also been adopted as intercalants to manipulate the stoichiometry and band structure.[25]

Sha et al. have reported detailed studies of H atom adsorption into the α-MoO_3 crystal lattice using density functional theory (DFT).[11] They have demonstrated that the adsorbed H atoms forms hydrogen molybdenum bronzes (H_x MoO_3) and the bandgap of such structures shift to metallic upon a hydrogen loading of $x > 0.25$ (**Figure 2**a,b). Practically, hydrogen adsorption can be induced by the breakdown of gas phase H_2 onto the MoO_3 surface, as well as electrochemical or chemical H^+ ions diffusion in liquid media into its lattice.[2,23] Figure 2c illustrates the experimentally calculated bandgaps estimated from the transmission spectral measurements. The inset shows the reduction in the bandgap value with respect to H_2 exposure time. Through Raman spectral studies, it was observed that at saturated levels of H intercalation, the diffused H atoms bond with oxygen atoms to form water vapor that leaves oxygen vacancies behind.[2,23] The formation of oxygen vacancies also reduces the bandgap of MoO_3, and partially reduced Mo^{5+}, Mo^{4+} states in the sub-stoichimetric $MoO_{(3-x)}$ lattice are established. Electrons from such reduced Mo ions give rise to gap states in between the valence and conduction bands, hence narrowing the bandgap.[2,24] A wide range of processes such as thermal treatment, UV irradiation and photochemical deposition followed by annealing can be adopted in achieving the aforementioned structural changes.[24,26]

MoX_2: In bulk form 2*H*-MoX_2 compounds are indirect bandgap materials with bandgap values of <1.3 eV as presented in Table 1. A general trend in the magnitude of the bandgap energies is observed as a decrease on going from sulphide to telluride. However, when the crystal thicknesses are reduced down to one layer, the bandgaps widen. Interestingly, they transform from indirect to direct bandgaps in this transition.

Kumar et al. have conducted first principles calculations of the electronic structure of both bulk and monolayers of MoX_2 compounds, which are presented in Figure 2d.[6] Such calculations generally show that the density states around the Fermi level are mainly due to the molybdenum *d* states.[6] The calculations also show a strong hybridization between molybdenum *d* states and chalcogen *p* states below the Femi level. The calculations also show that the transition of the band structure from indirect to direct bandgap, when reducing the slab thickness from bulk to monolayer, is due to changes in hybridization.[7] The energy bandgap of the monolayers was observed to increase in comparison to those of their bulk counterparts. The transition from indirect to direct bandgap has also been experimentally demonstrated via photoluminescence studies of mono- and multi-layered MoS_2, which will be discussed later.[7,12,14]

Similar to graphene and MoO_3, band structures of multilayered MoX_2 can be manipulated via various physical and chemical methods. Ramasubramaniam et al. have demonstrated through DFT calculations, the tunability of the bandgap in bilayered 2*H*-MoX_2 using external perpendicular electric fields (bandgap values decrease with increasing electric field).[10] At electric fields above 3 V nm^{-1}, the structure shifts to become metallic in all MoX_2 compounds. The tunability of the bandgap by reducing the number of layers, or alternatively the application of external electric fields, presents the possibility for a wide range of applications for layered MoX_2 compounds in the field of optoelectronics. Similar to MoO_3, there are also recent reports on the chemical intercalation of MoS_2 using ions such as Li^+ to reduce the bandgap.[8]

2.2.2. Electronic Properties

In developing a field effect transistor (FET), several properties of the incorporated semiconducting materials are of utmost importance: (a) the bandgap value that governs transistor switching, (b) charge density that describes the number of available free charges for transconductance, and (c) carrier mobility from which the transconduction gain can be obtained.

The main advantage of 2D MT&Ds over graphene is the presence of natural bandgaps, which allow the fabrication of FETs with very low OFF currents. Bandgaps in the range of those comparable with silicon (1.1 eV) or slightly less are the most desired. As discussed in Section 2.2.1, the bulk layered MoX_2 structure provides such bandgaps. In monolayers of MoX_2, even though the bandgap increases, it is still within the viable range. However for MoO_3, the bandgap is around 3 eV; this could be reduced using methods that were described in Section 2.2.1.

The magnitude of charge density is also a vital factor for developing FETs. At room temperature, many intrinsic semiconductors have relatively low charge densities that are not sufficient for generating enough output current in FETs. Doping and intercalation procedures are routinely implemented to increase the desired charge density.

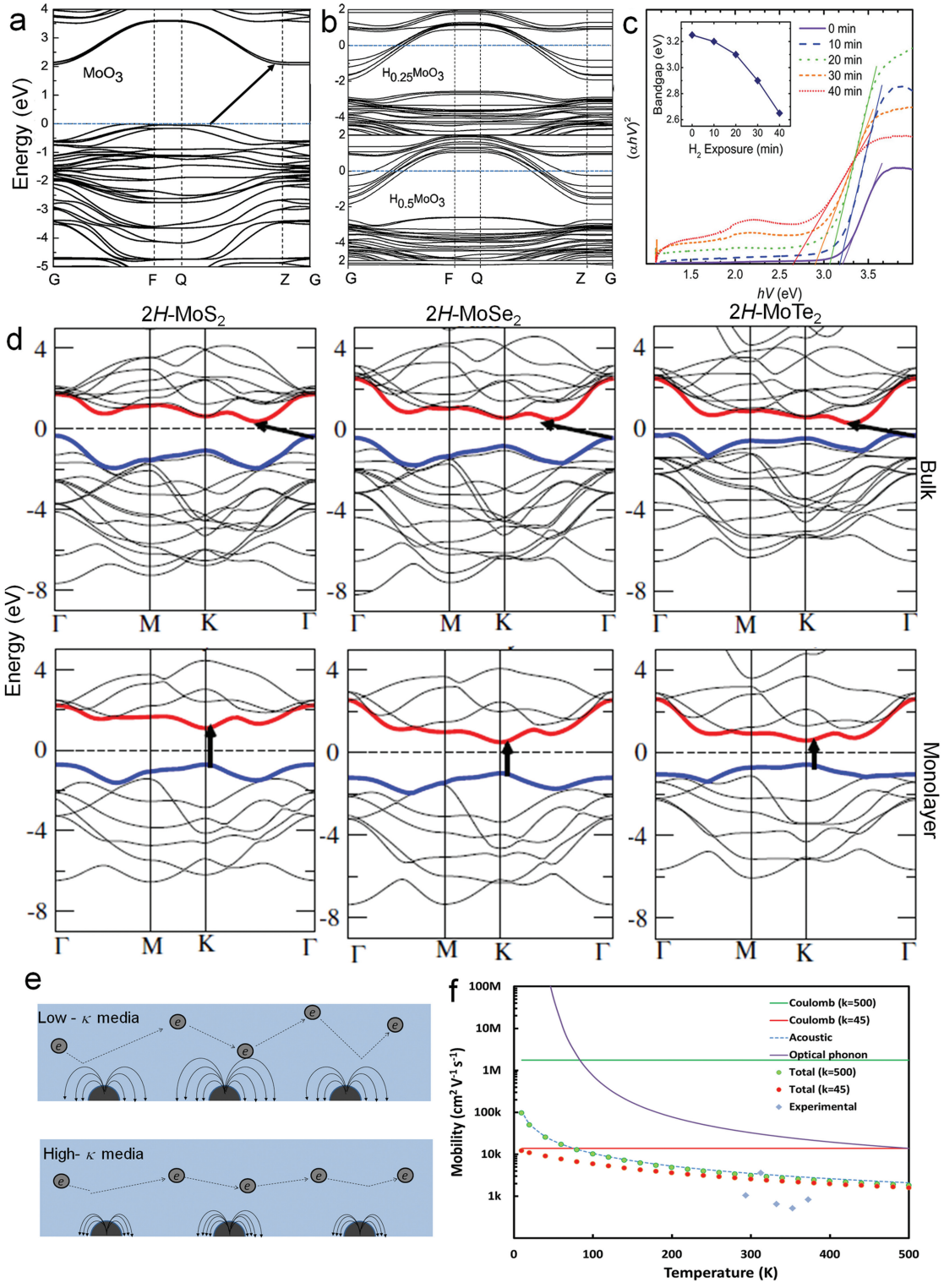

Figure 2. Band structure of a) α-MoO_3 and b) $H_x MoO_3$ ($x = 0.25$ and 0.5) obtained using DFT calculations. c) Photon energy vs $(\alpha h\nu)^2$ curves derived from the absorbance spectrum of a MoO_3 flake with progression of catalyzed H^+ intercalation. Intersection of the linear fit with the x–axis indicates the bandgap energy (inset: The change in estimated bandgap with progression of the intercalation process). d) Band structures of bulk and monolayer MoX_2 compounds. e) Illustration of a possible mean-free path for mobile carriers, affected by charge impurities in a low and high dielectric 2D medium. f) Theoretical calculations of charge carrier mobility affected by various scattering mechanisms as a function of temperature. The total mobility in a high-κ- and a low-κ 2D media comparable to the dielectric values of MoO_3 and MoS_2 are presented. Highest observed experimental carrier mobility values for MoO_3 and MoS_2 which closely match the theoretical predictions are also shown for comparison. a,b) Reproduced with permission.[11] Copyright 2009, American Chemical Society. c) Reproduced with permission.[2] d) Reproduced with permission.[6] Copyright 2012, Springer.

For the fabrication of FETs, enhanced charge carrier mobility in the semiconducting material is vital. In 2D MT&Ds, the charge carriers are confined within the layer that can potentially offer increased mobility. However, this carrier mobility in the 2D materials is also influenced and reduced by various charge scattering effects such as: (a) Coulombic, (b) optical phonon, (c) acoustic and (d) surface roughness.[27]

Coulomb Scattering: Coulombic scattering is caused by random charge impurities located within or on the surface of the 2D layer. The scattering from these charged centers in the electric quantum limit was first formulated by Stern and Howard in late 1960s.[28] As discussed in Section 2.2.1 in MD&Ts, Coulombic charges, such as the ionic intercalants, can be used in order control the size of the energy bandgap. This increases the charge densities, which is also desirable. However, the process also leads to increased Columbic scattering effects, potentially reducing the carrier mobility.

Polar Optical Phonon Scattering: In compound semiconductors, where the bonding is partially ionic, a polarization field arises.[27] The polarization field, forced into effect by the longitudinal-optical mode, causes a polar-optical interaction with the electrons, which scatters them and subsequently decreases their mobility.

Acoustic Phonon Scattering: Acoustic phonons operate via the generation of deformation potentials, which interact with charge carriers. These phonons produce crystal lattice deformations, which in turn produce localized electric potential affecting such carriers.

Surface Roughness Scattering: The influence of the surface or interface roughness on the mobility of 2D electrons has never been precisely assessed since the roughness behavior is never quite clear. For calculations, generally the surface fluctuations are assumed to be randomly correlated spatially, with a correlation that follows a Gaussian distribution.[29] In this case, two perturbation parameters influence the scattering mechanism: the random fluctuations in thickness and the correlation length (or average distance) between two roughness centers. Minimizing these parameters with perfect lattice matching between the 2D MT&Ds and their substrates have been suggested as possible methods to reduce the roughness scattering effect.

The carrier mobility in a thin layer is calculated using $\mu = \frac{e}{m^*}\langle\tau\rangle$ in which e is the point charge and τ is the transport relaxation rate of momentum in the (x, y) plane and m^* is the effective electron mass. Using the Born approximation, the transport relaxation time is calculated as:[27]

$$\frac{1}{\tau(E_k)} = \frac{2\pi}{\hbar}\sum_{k_z}\sum_{\mu}\int_{-\infty}^{+\infty} N_i^{(\mu)}(Z)\left|V_{k-k_z}^{(\mu)}(Z)\right|^2 \times (1-\cos\theta_{kk_z}) \times \delta(E(k)-E(k_z)) \quad (1)$$

in which $N^{(}\mu)_i$ (Z) is the concentration of the μ-th kind of charge center within the volume of $dxdydz$ and θ_{kk_z} is the angle between k and k_z vectors. In addition, $V_{kk_z}^{(\mu)}(Z)$ is an important parameter that shows the intensity of scattering and is described as the matrix element of the scattering potential. It is a potential function that describes the intensity of the scattering effect on free carriers. By correctly estimating the scattering potential, the transport relaxation rate and the associated mobility can be calculated. The overall carrier mobility can then be obtained using Mattheissen's Rule:[27]

$$\frac{1}{\mu_{TOTAL}} = \frac{1}{\mu_C} + \frac{1}{\mu_{PO}} + \frac{1}{\mu_A} + \frac{1}{\mu_{SR}} \quad (2)$$

where μ_{TOTOAL} is the overall mobility and μ_C, μ_{PO}, μ_A, μ_{SR} are the effective carrier mobilities limited by Coulombic, polar optical phonon, acoustic phonon and surface roughness scattering mechanisms, respectively.

Generally, Coulombic scattering is the dominant effect in reducing the overall charge carrier mobility at room temperature or below, for 2D materials such as graphene or MoS_2.[2,5] According to Equation (1), to tackle this, an increase in the dielectric constant is needed. The increase in the dielectric constant (electrical permittivity) of either the surrounding environment or the 2D material reduces the Coulombic effect as it confines the electric field generated by the Coulombic charges within smaller regions; hence, there is less of an effect on mobile charge carriers (Figure 2e). Dielectric constant (κ) engineering has proven to be effective in enhancing the charge carrier mobility.[2,5,30] The change in free carrier mobilities as a function of temperature and scattering parameters in a high dielectric 2D $MoO_{(3-x)}$ layer ($\kappa > 200$) are calculated using the Born approximation equation and presented in Figure 2f. As can be seen, due to the effect of a high dielectric constant, Coulombic scattering dominates at temperatures below 100 K, and above these temperatures, acoustic scattering effects is the limiting factor for the overall mobility. In the case of MoS_2 ($\kappa \approx 5$), the theoretical carrier mobility is still dominated by Coulombic scattering at room temperature, and the mobilities agree with the commonly observed experimental values.[5,31]

2.3. Optical Properties

Many 2D materials offer extraordinary optical properties that may be layer dependent. As mentioned previously, for MoX_2 the bandgap changes from indirect to direct, when the thickness is reduced to only one layer. As such, monolayer MoX_2 exhibits strong fluorescence. We have already discussed in Section 2.2.1, that bandgaps are intercalation dependent for both MoO_3 and MoX_2, as well as layer thickness dependent for MoX_2, which allows for the development of optical devices at various wavelengths. Similar to graphene, the Raman spectra of MT&Ds are also layer dependent, which also show strong changes of vibrational photospectroscopy upon intercalation and doping.

MoO_3: Raman vibration modes and chromism of α-MoO_3 are affected by intercalating ions. **Figure 3**a,b illustrate a mechanically exfoliated MoO_3 flake being intercalated with H^+ and its corresponding Raman spectra. For non-intercalated α-MoO_3, the chain of octahedral MoO_6 adjoined at the corners by a double-coordinated oxygen (Mo–O–Mo) stretching mode is assigned to the dominant 821 cm^{-1} peak. The edge-sharing triple-coordinated oxygen ($Mo_{(3)}$–O) stretching mode is reflected at 666 cm^{-1}, while the terminal oxygen (Mo–O) stretching mode is assigned to the peak at 996 cm^{-1}.[32,33] Peaks in the range of 100 to 500 cm^{-1}, resulting from various other

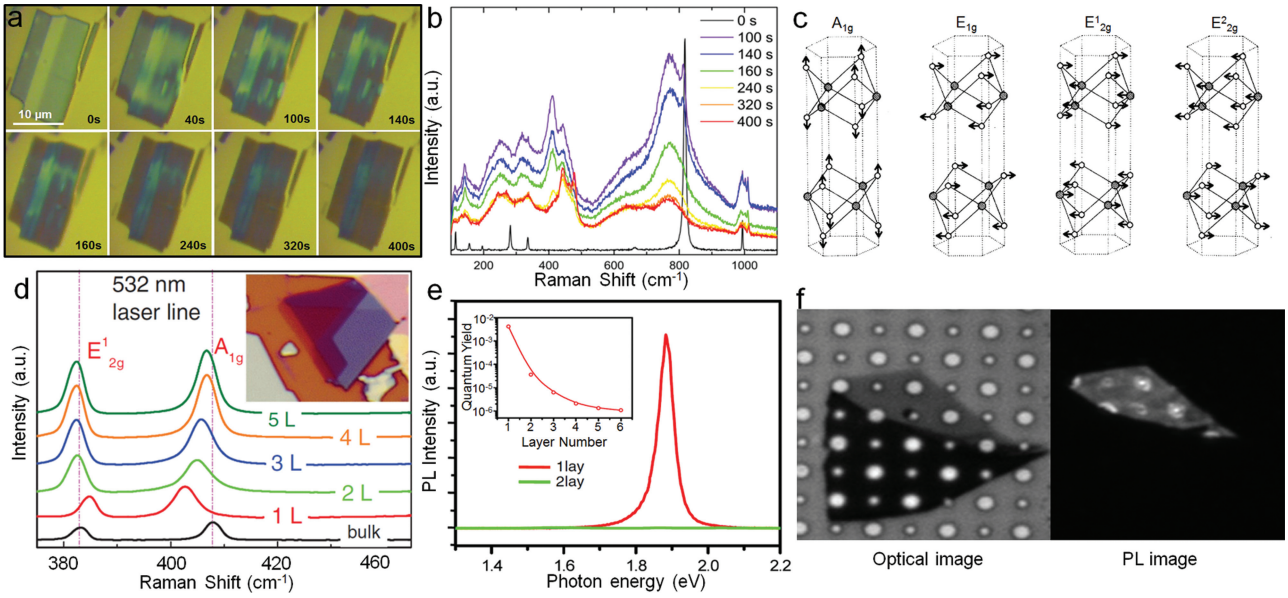

Figure 3. a) Optical microscope images and b) the corresponding Raman spectral evolution of an α-MoO_3 flake with the progression of H^+ ion intercalation. c) Raman active modes of *2H*-MoX_2 compounds. Dark shaded circles represent Mo atoms and the light circles represent chalcogen atoms. d) Raman spectra of MoS_2: from bulk to mono layers. e) PL spectra of a mono and bilayer MoS_2 flake with inset showing the variance of quantum yield with increasing number of layers. f) Optical image of a mono and multilayer MoS_2 flake in a silicon substrate with etched holes of 1 and 1.5 μm in diameter and its corresponding PL image. a,b) Reproduced with permission.[2] c) Reproduced with permission.[34] Copyright 1982, American Physical Society. d) Reproduced with permission.[38] e,f) Reproduced with permission.[7] Copyright 2010, American Physical Society.

vibrational modes such as scissoring, twisting and bending, can also be observed.[23] The strong coloration that originates from the edges and rapidly progresses towards the middle, caused by the intercalation, can be observed in Figure 3a. The Raman spectra also show that the peaks have broadened and intensities have greatly reduced along with the intercalation process. It has been suggested that this is due to the large lattice expansion and structural distortion related to interlayer H^+ intercalation.[32] Raman peaks corresponding to H_x MoO_3 and $MoO_{(3-x)}$ were identified similar to observations made by Ou et al.[23] Peaks shifts observed at 1010, 990, 810, 316, 140, and 112 cm^{-1} are due to the change in the force constants of the bonds related to the presence of H_x MoO_3.[23,32] Other peaks seen at 718, 436, 407, and 246 cm^{-1} can be assigned to various deformation modes of Mo and O bonds.[23]

Chromism in MoO_3 is achieved upon intercalation of ions that change the bandgap value. By reducing the bandgap, the appearance of MoO_3 changes from transparent to Prussian blue. This aspect can be utilized in optical applications, which will be described in Section 5.2.

MoX_2: Figure 3c illustrates the Raman active modes and Raman peak values for all the MoX_2 compounds (details presented in Table 1). The A_{1g},E_{1g} and E_{2g} correspond to the Raman active modes.[34,35] Out of those, E_{2g} is a low frequency rigid layer mode, which reflects the van der Waals binding forces between planes. By reducing the thickness of MoS_2 to a monolayer, Raman peak shifts appear in comparison to its bulk counterpart (Figure 3d). The shifts are observed in the two major modes of MoS_2, $E^1{}_{2g}$ and A_{1g}. For the $E^1{}_{2g}$ mode, the vibrations of both Mo and S atoms are limited to the horizontal plane, whereas for the A_{1g} mode, the displacements of S atoms are along the vertical plane.[36] For monolayers of MoS_2, the Raman peak shifts associated with $E^1{}_{2g}$ and A_{1g} modes are observed at 387 and 403 cm^{-1}, respectively.[37,38] Along with an increase in the number of layers, the frequency of the A_{1g} mode is observed to increase, whereas the $E^1{}_{2g}$ mode is observed to decrease in frequency.[37–39] This indicates stiffening of the A_{1g} mode, which is expected with an increase in the number of layers, causing increased van der Waals forces, which in turn suppresses the atomic vibrations along the vertical plane.[37,38] Above five layers, both vibrational modes seem to converge to their bulk values.[37–39] Such thickness dependent Raman peak shifts offer an effective method for identifying the number of layers (which will be further discussed in Section 4.2.).

Monolayers of MoS_2 exhibit a significant increase in photoluminescence (PL) in comparison to their bulk structure, owing to the change in band structure from indirect to direct bandgap.[7,12,14] Figure 3e illustrates the PL spectra of mono- and bi-layer flakes with the inset showing the apparent reduction in quantum yield with an increasing number of layers. Figure 3f shows the optical images of mono- and multi-layer flakes on a silicon substrate and its corresponding PL images. It should be noted that the enhanced PL emission from the monolayer is visible and the emission from the multilayer is too weak to be observable in the PL image.[14] The PL effect can be potentially used in many optical devices and sensing applications as will be presented in Section 5.7.

2.4. Mechanical Properties

In addition to all the exciting electronic and optical properties that 2D MT&Ds possess, understanding their mechanical properties is also of significant importance in the development of flexible mechanical devices and actuators. Bertolazzi et al. have demonstrated the strength and elasticity of suspended monolayers of MoS_2 to be comparable to that of stainless steel.[40] Gomez et al. have shown their ability to withstand elastic deformations up to tens of nanometers without breaking.[41] The average Young's modulus of suspended MoS_2 nanosheets are observed to be 270–330 GPa (in comparison to 180 and 1000 GPa for stainless steel and graphene, respectively).[40,41] These favorable mechanical properties also allow composite materials with MoS_2 nanosheets acting as reinforcing elements. Additionally, the elasticity of MoS_2 nanosheets readily exceeds those of flexible polymer thin films such as polyimide and polydimethylsiloxane (PDMS), which are commonly used in flexible electronics and microfluidics.[40] Interestingly, MoS_2 monolayers show a transition in electronic properties from semiconducting to metal in the presence of mechanical strain.[9,42] They change from direct to indirect bandgaps at small tensile strain (<2%) and shift into the metallic regime, before reaching the set tensile strength.[42]

MT&Ds can also show modest piezoelectricity in 2D form. From first principles studies, Duerloo et al. have reported on the intrinsic piezoelectric nature of monolayer MoX_2 compounds in contrast to their bulk counterparts.[43] Monolayer MoX_2 crystals are found to be non-centrosymmetric, whereas the multilayers possess a centrosymmetry with an inversion center.[43] The general trend is an increase in piezoelectric strength going from sulfide to telluride.

The elastic stiffness coefficients and the piezoelectric coefficients of MoX_2 compounds are summarized in Table 1. Such properties of 2D semiconducting materials can be potentially utilized in pressure and acceleration sensing applications as well as nanoelectromechanical systems.

2.5. Thermal Properties

Thermal conductivity of layered materials is directionally oriented. It has been shown that for MoS_2, the thermal conductivity along the plane is 18.06 W m^{-1} K^{-1}. Interestingly, this thermal conductivity drops to only 4.17 W m^{-1} K^{-1} for the out of plane direction.[44] Obviously, exfoliation and restacking of the layers reduce this thermal conductivity as they cause lattice mismatch, which promotes phonon scattering.[45] The relatively low thermal conductivity of the exfoliated MoX_2 group (Table 1), make them excellent candidates for thermally insulating solid lubricants. The changes in the thermal conductivity of MoS_2 and $MoSe_2$ with temperature are shown in **Figure 4**a. As can be seen, they all decrease with increasing temperature, which can be associated with the lattice vibrations at higher temperatures.

The variations in the Seebeck coefficients of pristine and exfoliated $MoSe_2$ as a function of temperature are shown in Figure 4b, for which both show increasing trends.[45] Such an increasing trend is commonly seen in all chalcogenide compounds. Seebeck values for the MoX_2 compounds are summarized in Table 1.

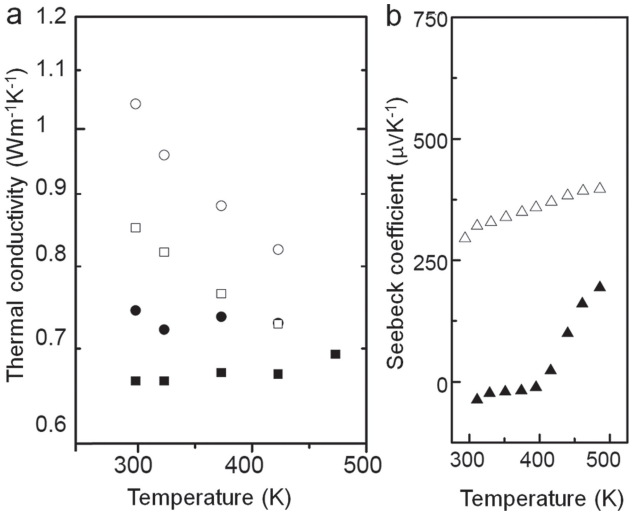

Figure 4. a) Thermal conductivities of MoS_2 and $MoSe_2$, b) Seebeck coefficient of $MoSe_2$ as a function of temperature. MoS_2 (circle), and $MoSe_2$ (rectangle) - Solid symbols indicate exfoliated and restacked compounds while open symbols indicate the pristine. Reproduced with permission.[45] Copyright 2010, Korea Chemical Society.

2.6. Magnetic Properties

The magnetic behaviors of MoX_2 and MoO_3 monolayers have not been experimentally studied. However, recent theoretical work by Ma et al. estimated the magnetic properties of 2D MDs with and without defects using density functional calculations.[46] They looked at cation and anion vacancies, as well as the related properties of 2D MDs with adsorbed atoms such as H and F. They demonstrated that only the cation vacancies can induce spin-polarization in $MoSe_2$ monolayers. They also suggested that the monolayers could potentially show long-range antiferromagnetic ordering after H atom adsorption into $MoSe_2$, and $MoTe_2$ and F atom adsorption into $MoSe_2$. This area will certainly require future investigations.

3. Synthesis of Layered Crystals

Out of a wide range of approaches available to synthesize layered MT&Ds, we have chosen some of the key methods to present here. We have classified them into three major categories, vapor, liquid and solid phase deposition techniques. The main foci of such synthetic processes include: increasing the planar area of the preferred growth of the layered material, control over the thickness, obtaining perfect crystallinity along the planes and possibly high yield.

3.1. Vapor phase Deposition

Vapor phase synthesis methods can be divided into two different categories: (i) physical vapor deposition (PVD) and (ii) chemical vapor deposition (CVD). Many PVD synthesis techniques such as thermal evaporation, molecular beam epitaxy (MBE), van der

Waal epitaxy (VDWE), pulsed laser deposition (PLD), electron beam evaporation (EBE), radio frequency sputtering (RFS) and direct current sputtering (DCS) have been used for the deposition of MT&Ds. However, most of these techniques (PLD, EBE, RFS) have been reported to produce MT&Ds in morphologies other than layered (e.g., nanoparticles, nanorods and nanotubes).[47] This is mainly due the fact that such approaches produce many nucleation sites and the resultant film growth is initiated from these sites. MBE and VDWE, at very low vacuum and controlled deposition rates, produce ordered layered structures.[48] However, MBE and VDWE have low deposition rates and are generally very expensive.

Amongst the PVD methods, thermal evaporation has so far been the most common and desired technique in synthesizing MoO_3, due to the ease of control over the deposition parameters by regulating the temperature and the carrier gas flow. Generally the process of Mo or MoO_3 powder sublimation occurs at >750 °C and the re-deposition takes place at locations with the base temperatures of <600 °C in the presence of carrier gases such as argon or oxygen.[2,3,33,49] Various morphologies and crystal phases are observed in the base temperature range of 400–600 °C, and the much desired large area layered crystals are obtained at around 550 °C (**Figure 5**a,b).[2] Due to the relatively higher sublimation (1100 °C) and lower oxidizing temperatures, synthesis of MoX_2 compounds via thermal evaporation has been generally disregarded.[50] There are reports on forming layered MoX_2 compounds under temperature controlled evaporation using stoichiometric amounts of the elements in powder form.[51,52] However, such approaches could be considered inefficient, since the reactions typically occur at very high temperatures in evacuated tubes, over several days.[52]

Carbonyl precursor assisted low temperature CVD has been demonstrated in the synthesis of α-MoO_3.[53] Additionally, chemical transport reactions followed by post annealing have been reported to produce α-MoO_3 thin films.[54] These techniques have been mainly adopted in the production of large area MoO_3 thin films for chromogenic applications such as smart windows.[54] CVD methods also offer excellent alternatives to thermal evaporation in synthesizing layered MoX_2 compounds. Evaporation of Mo and annealing under hydrogen disulfide (H_2S) has been reported to produce atomically thin MoS_2.[55] However, the resultant growth has been observed to produce nanoclusters. Direct sulphurization of evaporated Mo,[56] or α-MoO_3 powder,[50,57] could be considered as the simplest CVD approach for synthesizing layered MoS_2, as it also assists in forming the preferred layered structure. The experimental setup depicting the simultaneous evaporation techniques for MoO_3 nanopowder, along with pure sulphur powder is illustrated in **Figure 6**a. The resultant thin film growth has been observed to form layered crystalline *2H*-MoS_2 platelets.[50] The challenge here is to synthesize these layered crystals into large areas for electronic applications. In another approach, the initial MoO_3 precursor was first evaporated onto wafers in nano-meter thicknesses, reduced using H_2 gas and then sulphurized.[58] Figure 5d,e present high resolution transmission electron microscopy (HRTEM) images of a monolayer MoS_2 sheet obtained from the aforementioned methods, indicating the horizontal lattice spacing.[57]

Diskus et al. have demonstrated the synthesis of layered α-MoO_3 thin films using commercial molybdenum hexacarbonoyl

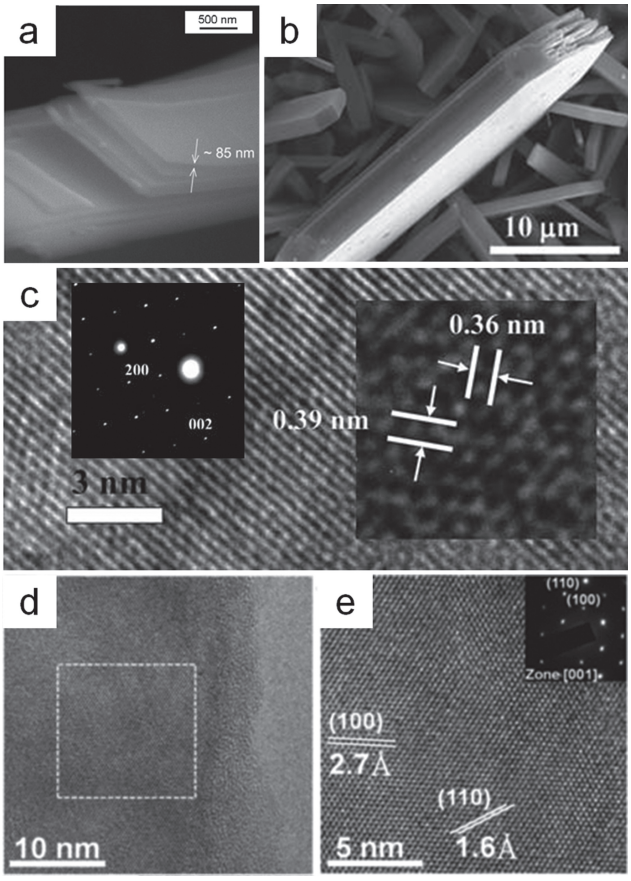

Figure 5. Magnified scanning electron microscope (SEM) images of α-MoO_3 a) nanobelts and b) large area layers acquired via thermal evaporation technique. c) HRTEM image of the crystals seen in (b). Inset: selective area electron diffraction (SAED) pattern and magnified HRTEM indicating the lattice spacings of atomically thin α-MoO_3. d) HRTEM image of MoS_2 monolayer. e) Enlarged HRTEM image of the marked area in (d), with an inset showing the SAED pattern. a) Reproduced with permission.[33] Copyright 2009, Elsevier. b) Reproduced with permission.[3] Copyright 2009, Royal Society of Chemistry. d,e) Reproduced with permission.[57]

($Mo(CO)_6$) as a precursor, via an ALD technique.[59] The thickness of the deposition on the substrates has been controlled through the number of deposition cycles at a particular temperature. The as-deposited samples were then annealed at 600 °C to obtain highly crystalline α-MoO_3. The synthesis of layered MoX_2 compounds through ALD has yet to be explored.

3.2. Liquid Phase Deposition

Liquid phase techniques include various methods such as electrodeposition, hydrothermal, and sol gel. In such methods, the ionic precursors containing Mo and oxygen or chalcogens are used. Upon applying suitable energy (electrical, heat or chemical), the target interactions occur and the layered MT&Ds form.

Synthesis of layered crystalline α-MoO_3 through electrodeposition of a sodium molybdate (Na_2MoO_4) solution followed by annealing has been reported (Figure 6b).[17] Deposition has

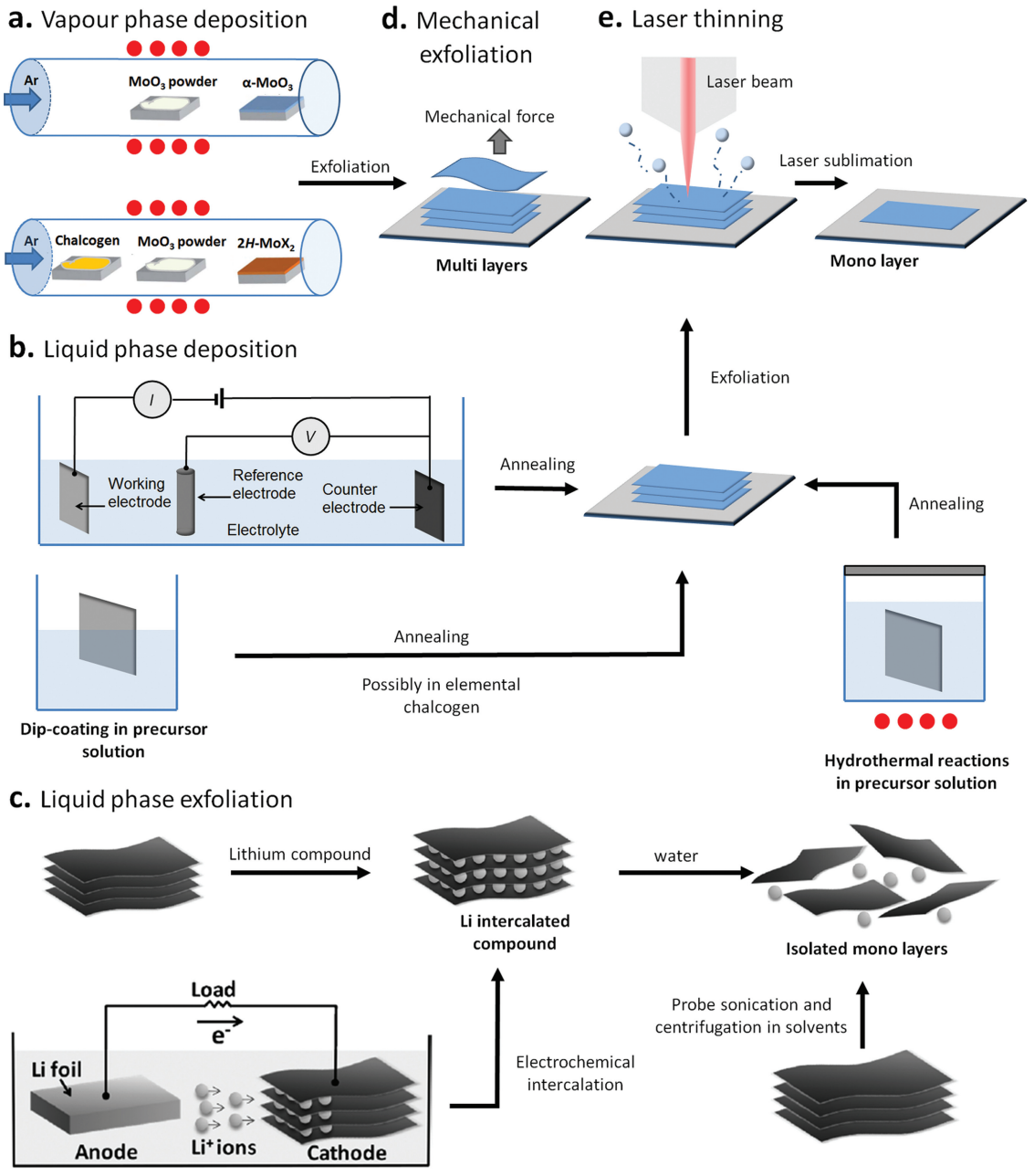

Figure 6. Illustration of the most simple and commonly adopted techniques, in producing 2D materials. a) Experimental setup illustrating the VPD technique: thermal evaporation of MoO_3 powder to produce layered α-MoO_3 and co-evaporation of MoO_3 and elemental chalcogen to produce layered *2H*-MoX_2. b) Liquid phase approaches in producing layered MT&Ds (electro-deposition, dip-coating and hydrothermal). c) Various liquid phase exfoliation routes adopted in producing 2D materials. Illustration of d) mechanical exfoliation and e) laser assisted sublimation approaches utilized in producing 2D systems. c) Reproduced with permission.[71]

been carried out under set pH (acidic) conditions at room temperature. The as-deposited samples were then annealed at 300 °C in ambient air to attain layered form crystalline α-MoO_3. Other reports include synthesis via alternate electrolytes and voltammetry conditions.[60]

Synthesis of α-MoO_3 has been hydrothermally conducted using various solutions containing chemical such as H_2O_2, polyethylene glycol and ammonium heptamolybdate.[61] Among the MDs, layered MoS_2 has been reported to be synthesized via hydrazine-assisted low temperature hydrothermal reactions between Na_2MoO_4 and $Na_2S_2O_3$.[62] Similarly, layered $MoSe_2$ has been produced by using Na_2SeSO_3 as the Se source. Later Peng et al. demonstrated the relatively large area synthesis of MoS_2 and $MoSe_2$ by adopting hydrothermal reactions between ammonium molybdate and elemental S and Se, respectively.[63] Other reports by Matte et al. have also included hydrothermal

synthesis of MoS_2 (MoO_3, KSCN as precursors) and $MoSe_2$ (MoO_3, Se as precursors).[64]

Sol–gel processing is a versatile technique for synthesizing MT&Ds. Prasad et al. have reported obtaining α-MoO_3 thin films via sol–gel processing, using 0.1 M molybdenum isopropoxide in n-butanol as the precursors in a nitrogen atmosphere (to avoid reaction with oxygen).[65] The thin films were prepared via ultrasonic agitation, and spin-coating followed by low temperature annealing.

Wet chemical approaches in producing monolayers of MoS_2 via low temperature thermal decomposition of a single source precursor containing both Mo metal and S have also been demonstrated.[66,67] In a wet chemical approach, ammonium tetramolybdate ($(NH_4)_2MoS_4$) has been stirred in oleylamine and allowed to decompose at elevated temperatures.[66] After cooling down, 2D MoS_2 nanosheets were obtained in suspension.

3.3. Solid-State Reactions

There are also alternative methods that have the potential to be further studied. Bonneau et al. reported on the production of layered MoS_2 and $MoSe_2$ through rapid solid-state reactions between molybdenum chlorides and alkali metal chalcogenides.[52] These vigorous reactions were observed to generate crystals instantaneously and the layered materials were simply separated by washing the end product. Such a process has not been used for directly forming exfoliated layers as of yet.

4. Exfoliation and Identification of Layers

After synthesizing layered MT&Ds using the aforementioned methods, they can be readily exfoliated into their 2D planar forms. This section focuses on such exfoliation approaches and additionally on the procedures that are involved in identifying the exfoliated planes and determining the number of layers.

4.1. Exfoliation Mechanisms

This section covers the primary approaches employed in the exfoliation processes of layered MT&Ds. Two broadly applied procedures include mechanical and liquid phase exfoliation. In addition, a recently reported method via exposure to laser beams will also be discussed.

4.1.1. Mechanical Exfoliation

Mechanical exfoliation is a simple technique that has become the most widespread process adopted for achieving monolayers since the discovery of graphene.[5,68] It involves the application of a mechanical force, e.g., using adhesive tape, to exfoliate the bulk materials into mono- as well as multi-layered flakes (Figure 6d). This process exploits the weakly bonded nature of the layers between the planes. Its main limitation is that it cannot be implemented on a large scale. Successfully achieving atomically thin layers of α-MoO_3 via the application of mechanical exfoliation has been demonstrated.[2,3] Many of the interesting properties and applications reported for monolayered MoS_2 have also been achieved through mechanical exfoliation.[5,14] Mechanical exfoliation can be considered to be the most effective technique in establishing proof-of-concept studies, as it produces high quality intrinsic 2D materials. However, for large scale fabrication of 2D devices, other options should be explored.

4.1.2. Liquid Exfoliation

Liquid phase intercalation/exfoliation approaches have been explored since the early 1970s.[69] Such techniques involve introducing guest species in-between the gaps of the host layered materials and then separating them using various ways (Figure 6c). One of the common intercalants used is lithium (Li).[12,64,70] Here, the layered materials are immersed into *n*-butyl lithium for a particular duration to allow consistent intercalation of Li. Water is then added to the lithiated material, where the intercalated Li vigorously reacts with water, producing lithium hydroxide and hydrogen gas, and separating the monolayers.[64] The disadvantage of this approach is that sometimes the intercalation process takes several days. Zhang et al. have demonstrated an electrochemical alternative that is faster and, at the same time, offers control over the degree of the lithiation (Figure 6c).[71] The intercalation process is controlled by monitoring the galvanostatic discharge in the setup.

Re-aggregation after removing ions can be considered as one of the major disadvantages faced in intercalation-based exfoliation techniques.[72,73] However, Eda et al. have reported the restoration of exfoliated monolayers back to their pristine semiconducting state by mild annealing above 300 °C.[12] Coleman et al. have recently demonstrated exfoliation of layered materials in organic solvents and with aqueous surfactant solutions.[73,74] Here, the layered materials were sonicated in a range of solvents and then centrifuged. The separated supernatant from the centrifuged dispersion was then filtered to obtain exfoliated layers. Furthermore, Yao et al. have demonstrated low energy ball milling followed by sonication in the production of large area 2D sheets.[75] Although the quality and the degree of exfoliation in such solvent-based approaches are not high, they can provide large area thin films.[73]

4.1.3. Laser Thinning

Steele et al. have reported a novel method for obtaining monolayers of MoS_2 using laser exposure.[76] This process depends on the sublimation of MoS_2, triggered by heating. In layered materials such as MoS_2, the van der Waals gap plays a very weak role in dissipating the laser induced heat, hence, sublimating only the top layers in a multi-layered flake is possible (Figure 6e). Interestingly, the perfect contact between the monolayers and the substrate provides a conduction path to dissipate the heat through the substrate, leaving the bottom monolayer intact (refer to **Figure 7**a,b for optical images).[76] Utilizing this method, the authors have also demonstrated the fabrication of monolayers in arbitrary shapes, with the smallest feature size reaching approximately 200 nm.[76] Such a technique can potentially be adopted for the large-scale fabrication of electronic devices based on 2D materials.

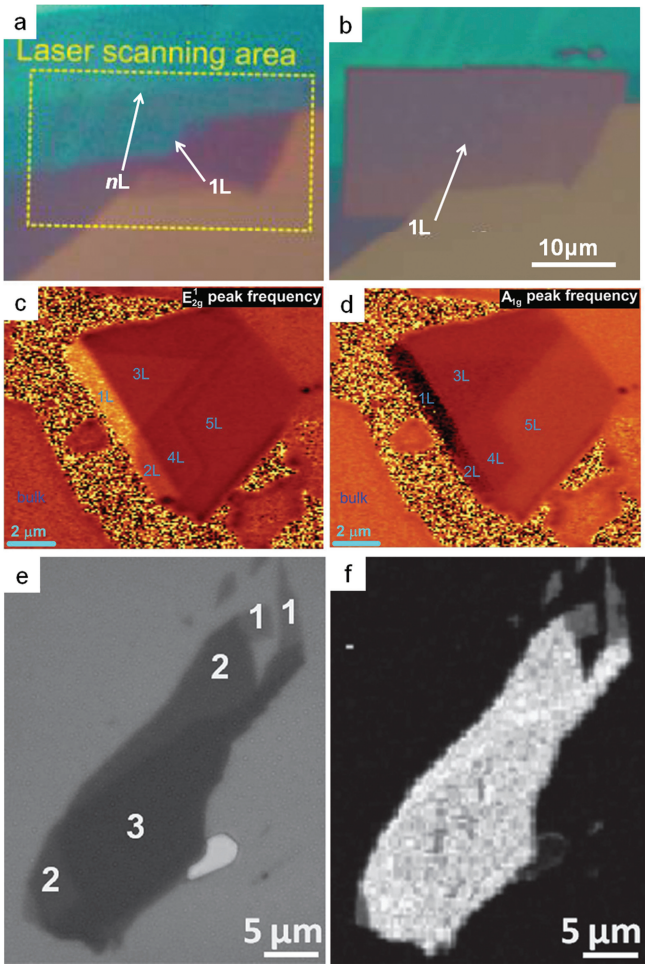

Figure 7. a) Optical microscopy image of a multilayered MoS_2 flake exfoliated onto a SiO_2/Si substrate. b) Same as in (a) after laser scanning in the area marked by the dashed rectangle in (a). Raman peak frequency map of c) E^1_{2g} mode and d) A_{1g} mode of a multi layered MoS_2 flake. e) Monochromic red channel optical microscope image of a few layer MoS_2 and f) its corresponding Raman peak frequency mapping for comparison. a,b) Reproduced with permission.[76] Copyright 2012, American Chemical Society. c,d) Reproduced with permission.[38] e,f) Reproduced with permission.[77]

4.2. Identifying Monolayers

Following exfoliation, identifying the number of layers in the 2D MT&Ds is a crucial step. Simple techniques for identifying monolayers are required to increase efficiency of the process. Mechanical procedures such as scanning probe microscopy (SPM) and atomic force microscopy (AFM) have already been established in identifying such thin layers.[68,77] They have a resolution of <0.02 nm that can be readily used for measuring step changes as small as 0.6 nm, which are on par with the fundamental thicknesses of MT&D monolayers.

As discussed in Section 2.3, Raman spectroscopy is an excellent tool for identifying the layer dependent bond vibrational distinctions caused by lattice structural variations. The ability to map the wavenumber of the thickness dependent Raman vibration mode (E^1_{2g}), offers a method to accurately identify the number of MoX_2 layers. Interestingly, the A_{1g} mode is also dependent on the number of layers. Figure 7c,d illustrate the wavenumber map of E^1_{2g} and A_{1g} modes of a multi-layer MoS_2 flake.[38] Note that the E^1_{2g} map provides much greater clarity compared to the A_{1g} map, in distinguishing between the number of layers (compare Figure 3d insets: Optical microscopic image of the corresponding flake).[38] Raman micro-spectroscopy could be highly useful in identifying the number of layers in small area flakes with a spatial dimension that can be as small as 250 nm.

Optical microscopy is the most commonly adopted technique for identifying the number of layers of large area coverage. In general, the material is exfoliated onto silica on silicon (SiO_2/Si) substrates with a specific SiO_2 thickness (270 to 300 nm). Different layer thicknesses are then identified by comparing the optical color contrast to previously benchmarked thicknesses.[77] However, in certain cases the optical contrast between monolayer, bilayers and tri-layers tend to be ambiguous. Zhang et al. have reported an easier solution utilizing optical microscopy in combination with image analysis software (IMAGE J).[77] Here, optical microscope images of multilayered flakes are obtained, and the color image is then split into three monochromic red (R), green (G), and blue (B) channels. Figure 7e,f show an R-channel image of a multilayer large area MoS_2 flake and the corresponding Raman frequency mapping. The intensity difference between the MoS_2 layers and the substrate was observed to be increasing with the number of layers.[77]

5. Applications

5.1. Lubricants

The lamellar crystal structure seen in naturally occurring compounds such as micas and graphite are desirable for lubrication applications. Similarly, layered MoX_2 and MoO_3 are excellent candidates due to their lamellar structure and the weak attraction between the planes, which are governed by van der Waals forces. Hence, any small shear force applied along these planes can slide layers on top of each other.[78,79] The drawbacks of MoX_2 and MoO_3 based lubricants are that they are sensitive to environmental factors (humidity and oxygen) and their hardness is relatively lower than competing lubricants.[78,80] Generally doping of such compounds reduces their sensitivity to the environment, and enhances their load bearing capacity and wear resistance.[81] In general, MoX_2 compounds are excellent lubricants in vacuum or non-oxidizing environments.

MoX_2 compounds are generally used either as an additive in liquid media[82] or as a solid lubricant coating.[78,83] Sputtered MoS_2 and $MoSe_2$ on various metal substrates have been reported to show excellent performance as solid lubricants with better stability than $MoTe_2$.[78,83] Recently Martin et al.[84] have demonstrated superlubricity with coefficients of friction on the order of 10^{-3}, which is attributed to the interlayer Coulombic repulsive interactions in the lattice.[79] Oxidizing behavior of MoX_2 compounds in lubricant applications has been reported to degrade the lubrication properties at temperatures exceeding 500 °C,[78] possibly due to the formation of non-layered crystal structures.

5.2. Electrochromic Systems

Layered MoO_3 electrochromic (EC) based systems, such as smart windows and optical displays, have been studied for more than three decades.[85] In these systems, the optical transparancy of MoO_3 can be switched reversibly and persistently in the presence of an electrolyte containing positive ions such as H^+, Li^+ and Na^+ by applying low voltages*vs.* a reference electrode. As described in Section 2.3, the origin of the variation of the optical properties in MoO_3 is ascribed to the valence state transition of MoO_3 from 6+ (transparent) to 5+ (Prussian blue) upon positive ion intercalation.

Although 2D structure facilitates the spill-over of positive ions along the planes, which enhances the ion intercalation kinetics, such an advantage is offset by the smaller surface area in comparison with those of nanoporous surfaces. Ideally, the most efficient system can be made of layered films with planes normal to the surface of the electrodes, which is a challenging task to construct. To date, the best coloration efficiency obtained by MoO_3 nanostructures is only up to 46.2 $cm^2\ C^{-1}$, which is only one-third of the best of those made from WO_3 nanoporous structures (141.5 $cm^2\ C^{-1}$).[86] Composite MoO_3–WO_3 thin films with coloration efficiencies up to 120 $cm^2\ C^{-1}$, with high transmittance and good cyclic stability, have also been reported.[53] On the other hand, MoX_2 are generally not considered as electrochromic materials as their valence states are stable at 4+, which are almost impossible to be reduced to +3 in order to induce coloration.

5.3. Electronic Devices

As presented in Section 2.2.2, both 2D MoX_2 and MoO_3 have been favorite candidates in the fabrication of electronic components, especially FETs. As discussed earlier, the ease of manipulation of the electronic properties through ionic doping and other approaches, reasonable charge carrier mobility due to quantum confinement and the possibility of making both Schottky and ohmic contacts in the vicinity of metals make 2D MT&Ds favorable for the electronics industry.

One of the first reports on 2D MoS_2 is Novoselov et al. work on measuring room temperature carrier mobilities on the order of 0.5 to 3 $cm^2\ V^{-1}\ s^{-1}$.[4] More recently, Radisavljevic et al. demonstrated enhanced charge carrier mobility reaching values as large as ≈220 $cm^2\ V^{-1}\ s^{-1}$ for monolayered MoS_2, comparable to the values achieved in doped silicon thin films and graphene nanoribbons.[5] The use of a 30 nm thick HfO_2 layer as a high-κ dielectric top gate (**Figure 8**a) was the reason for such an increase as was comprehensively discussed in Section 2.2.2. The field effect characteristics of this monolayered MoS_2 transistor, obtained at different gate voltages are shown in Figure 8b,c. Remarkable drain-source current I_{ON}/I_{OFF} ratios of 10^6 and 10^8 for bias voltages of 10 mV and 500 mV, and OFF-state currents smaller than 100 fA indicate the high performance of the device. Such monolayer transistors connected in series have been further developed into simple logic operators, signal amplifiers and even more complicated integrated circuits such as static random access memory (SRAM) and five-stage ring

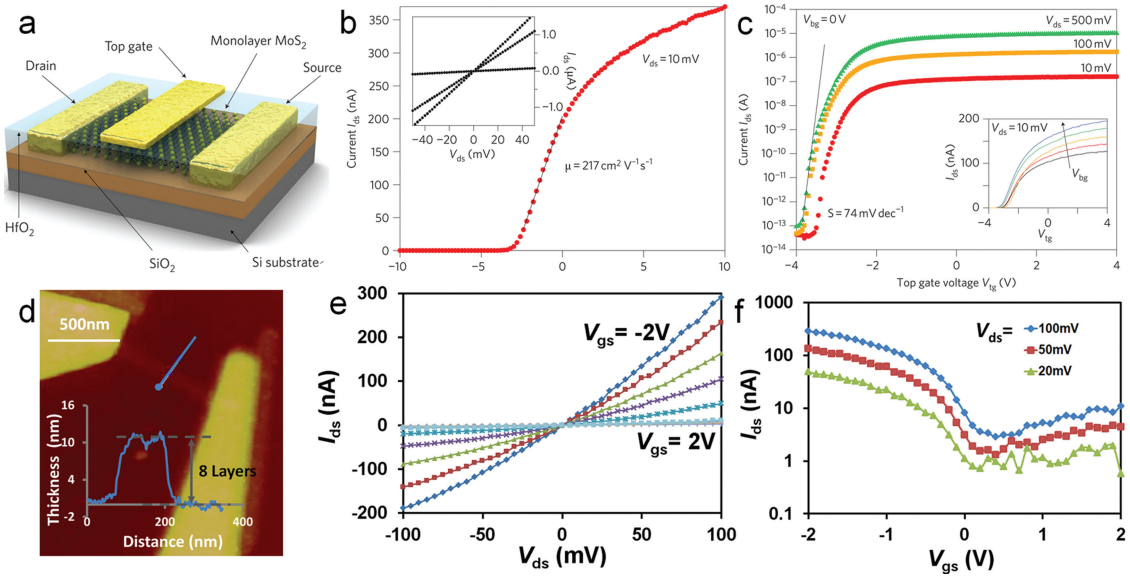

Figure 8. a) 3D Schematic illustration of a monolayer MoS_2 FET and b) its corresponding room temperature transfer characteristics, with inset showing drain-source current (I_{DS}) vs drain-source voltage (V_{DS}) curves for Back gate voltage (V_{GS}) values 0, 1, and 5 V. c) Field-effect measurements of MoS_2 monolayer based FETs. The I_{DS}–V_{TG} curves recorded for a bias voltage ranging from 10 to 500 mV showing ON/OFF ratios > 10^6. d) AFM scan of a FET fabricated with few layered $MoO_{(3-x)}$ and its the corresponding thickness profile. The measured thickness of ≈11 nm indicates the presence of eight fundamental layers. e) I_{DS} vs. V_{DS} characteristics of the $MoO_{(3-x)}$ FET with varying back-gate voltages (V_{GS}) in steps of 0.4 V from –2 to +2 V and f) the corresponding I_{DS}–V_{GS} curves acquired at V_{DS} values of 20, 50, and 100 mV. d–f) Reproduced with permission.[2] a–c) Reproduced with permission.[5] Copyright 2011, Nature Publishing Group.

oscillators.[87] Furthermore, substrate and gate dielectric engineering have also been proven to result in significant enhancement of carrier mobilities in multilayer MoS_2.[31,88] The main issue with MoX_2 based FETs is the intrinsic theoretical limitation of the carrier mobility in such materials that remains under 500 $cm^2\ V^{-1}\ s^{-1}$; this still cannot quite rival that of silicon.[5,31] However in a recent report, Das et al. have shown that eliminating the contact resistance effects through a novel selection of source/drain contacts can result in dramatic enhancement in carrier mobilities (700 $cm^2\ V^{-1}\ s^{-1}$) in thin layers of MoS_2.[89]

FETs incorporating ultrathin $MoSe_2$ layer, with mobilities of 50 $cm^{-2}\ V^{-1}\ s^{-1}$ and ON/OFF ratios $>10^6$ have been recently realized.[90] In addition to FET structures, Spah et al. have reported heterojunction diodes achieved through van der Waals epitaxial growth of a *n*-$MoSe_2$ on other *p*-type TMCs (WSe_2).[91] These structures have proven to be effective in diode applications since they present excellent lattice matching.

α-MoO_3 has been established as a real alternative in surpassing the charge carrier mobility values of silicon.[2] As described in Section 2.2.2, its intrinsic high-κ provides a natural environment that reduces the Coloumb scattering. An AFM image of such a reduced α-MoO_3 ($MoO_{(3-x)}$) based FET and its thickness profile can be seen in Figure 8d. Charge carrier mobilities exceeding 1100 $cm^2\ V^{-1}\ s^{-1}$ were realized in such structures fabricated on standard back gate SiO_2/Si substrates.[2] Figure 8e,f show the field effect characteristics obtained from this transistor. Relatively low I_{ON}/I_{OFF} ratios were due to the near metallic property of $MoO_{(3-x)}$ layers at the metal semiconductor interface. In addition, potassium intercalated (K_x MoO_3) single nanowire based ultra-sensitive phototransistors, with I_{ON}/I_{OFF} ratios up to 10^4 for a broad spectral range, have also been recently demonstrated.[92]

Another new application of MoS_2 has recently appeared in valleytronics, which involves channeling charge carriers into and out of valleys of set momentums.[93] The crystal structure of MoS_2 creates two momentum valleys that are not symmetric. By using polarized light, it is possible to nudge carriers preferentially into one valley state or another. Due to their fast response, such interactions can be used in super high rate electronic and optical switches.

The relative abundance of MT&Ds in nature, their high stability, and the ease of property manipulations, render 2D MT&Ds one of the most promising building blocks for future electronic systems.

5.4. Battery Electrodes

The electrochemical properties of layered MoX_2 structures as electrodes for lithium ion batteries (LIB) have also been of growing research interest. Once again the lamellar structure of MoX_2 aids in alkali ion insertion in between the inter-layer and intra-layer spaces of these crystals. Obviously, the large inter-planar space in an MoX_2 lattice would be favorable to fast lithium intercalation and high lithium storage capacity.[94] 2D MoS_2 obtained from exfoliation and restacking,[94,95] as well as solvothermal synthesis routes have been reported as electrodes for LIBs.[96] One of the major issues faced in the use of intrinsic layered MoX_2 in LIBs is the lack of cycling stability and rate capability limitations due to their proneness to very compact aggregation after repetitive cycles as well as the formation of gel-like polymeric layers due to electrochemically driven electrolyte degradation.[97–99] Such an issue can be suppressed via forming composites of 2D MoX_2 with other materials.[97] Recently, Chang et al. have demonstrated high reversible capacities and cycling stability in MoS_2/carbon-based (amorphous carbon and graphene) hydrothermally developed composites with uniformly dispersed 2D MoS_2.[98] Mono- and multilayered MoS_2/graphene composites were reported to have specific capacities as high as 1100 $mAhg^{-1}$ as well as excellent cycling stability.[97,100] MoS_2/reduced graphene oxide and mesoporous carbon composites have also been established as battery electrodes.[99,101] Furthermore there are also reports on the application of MoS_2 electrodes in Mg ion batteries.[102] In addition to MoS_2, other 2D MoX_2 compounds have also been used in LIBs. Morales et al. have successfully demonstrated the use of polycrystalline 2*H*-$MoSe_2$ as a cathode material in both lithium and sodium cells.[103]

The application of α-MoO_3 as a LIB electrode dates back to early 1970s. Its popularity has mainly been due to its lamellar structure and facile formation of intercalated states.[104,105] Detailed explanations on the structural evolution and intercalation of MoO_3 crystal lattice are discussed in Section 2.3 and also found elsewhere.[105,106] Similar to MoX_2 compounds, intrinsic α-MoO_3 is outperformed by composite electrodes and ion doped MoO_3 structures. Mai et al. reported electroactivity of α-MoO_3 nanobelts after lithiation, which showed superior performance in comparison to pristine α-MoO_3 nanobelts. Excellent cycling capabilities with capacity retention rate of 92% were observed in lithiated nanobelts, whereas the pristine samples only exhibited up to a 60% retention rate.[107] Reports of α-MoO_3 composite electrodes with various binders show their excellent electrochemical properties, while bio derived sodium alginate has emerged as the best performing binder with stable specific capacity of approximately 800 $mAhg^{-1}$.[108] Further studies have shown carbon and graphite coated α-MoO_3 composites exhibit the highest achieved electrochemical performance so far.[109] Tang et al. have demonstrated α-MoO_3 composites electrode based rechargeable LIBs with excellent retention rates and energy densities potentially suitable for large power systems.[110]

5.5. Catalysts

Layered MT&Ds have been widely used in catalysis in their pristine forms as well as doped and composite forms.[111] MoS_2 nanostructures have been commonly used as catalysts in catalytic reactions such as hydrodesulphurization (HDS) and more recently for hydrogen evolution reactions (HERs).[112,113] The catalytic activity is generally attributed to the unsaturated sites at the particle edge surfaces, parallel to the hexagonal axis of lamellar MoS_2 structures.[114,115] For HERs, a systematic investigation of surface sites on MoS_2 nanoparticles of Au (111) have revealed that hydrogen evolution correlates linearly with the number of edge site on the MoS_2 catalyst.[113] Hence, the key factors for optimization of the HER activity in MoS_2 are increasing the catalytic activity of the active sites, enhancing the number

of active sites (MoS_2 layer edges, therefore the applications of structures such as nanoribbons are advised) and increasing the electrical contact to the active sites (which is provided by the planar routes for electrons within the 2D structure). The integration of layered MoX_2 with the morphologically compatible graphene has also shown promise in increasing the catalytic activity. Li et al. have demonstrated that few layered MoS_2 structures synthesized on graphene sheets show enhanced electrocatalytic activity in HERs which has been attributed to the abundance of exposed MoS_2 edges on graphene and their excellent electrical coupling.[116] Additionally, exfoliated $MoSe_2$ has also been established as an electro-catalyst in $Pt/MoO_x/MoSe_2$ electrode structures.[117]

MoO_3 has been widely adopted as a catalyst in dehydrogenation of gaseous organic compounds. Monolayer molybdenum oxide on alumina (MoO_3/Al_2O_3) has been reported to be a good catalyst in the dehydrogenation of cyclohexene and pyridine.[118] Increased catalysis by alkali contributors in similar MoO_3/TiO_2 systems for dehydrogenation of propene has also been demonstrated.[119] Solid state catalysis based on MoO_3 has been reported to be a viable option for industrial scale formaldehyde production through the oxidation of gaseous methanol.[120] In addition, HDS catalysis and selective catalytic reduction based on MoO_3/Al_2O_3 and MoO_3/TiO_2 have been demonstrated.[121] Other reports include supported MoO_3 on metal oxides such as SiO_2, TiO_2, ZrO_2, and Nb_2O_5 adopted for various catalytic applications.[122]

MoX_2 and MoO_3 have also been incorporated as photocatalysts. The bandgap of MoO_3 is slightly larger than its more stable rivals such as WO_3 (≈2.7 eV).[19] As a result, despite showing promise, in its intrinsic form MoO_3 cannot surpass the performance of WO_3. Interestingly, using intercalation, the bandgap of MoO_3 can be reduced to cover a wide range of the visible and infra-red spectrum. Yet, much research needs to be conducted to obtain stable intercalated MoO_3 or WO_3 for such applications. Amongst MoX_2, MoS_2 has been increasingly studied in photocatalytic applications. The MoS_2 band position is slightly more positive than that for HER.[123] As such, MoS_2 is a possible candidate for HER, if only the conduction band can be pushed to slightly more negative values. This means that MoS_2 would only evolve hydrogen if quantum confinement is introduced.[124]

5.6. Optical Devices

Layered MoX_2 are possible candidates for developing different types of optical devices, including solar cells based on photoelectrochemical (PEC), junction and organic technologies, semiconducting optical devices such as photo- and light emitting diodes.

MoX_2 are used in PECs solar cells, due to their inherent resistive nature to photo-corrosion and energy bandgaps comparable to that of silicon that covers a large solar spectrum.[125] A good example is the work by Pathak et al. who developed $MoSe_2$ based PECs cells by dipping the semiconductor electrodes in an ionic electrolyte forming a Schottky interface around which the photo generated electrons are harvested. The efficiency of such PEC solar cells is still much lower than ideal. The best electrode structures are those consisting of large surface areas with paths of minimum charge carrier scattering to increase the efficiency. Obviously, the best candidates will be vertically oriented planes of MoX_2, which are still challenging to create.

MoS_2 has also been incorporated as counter electrode catalysts in dye-sensitized solar cells (DSSCs). Significant conversion efficiencies of up to 7.59% have been observed similar to that of DSSCs with Pt counter electrodes.[126] Composite structures such as MoS_2—carbon/carbon nanotubes, MoS_2—graphene nanosheets have also been established as Pt-free counter electrode in DSSCs.[127,128] Relatively higher conversion efficiencies achieved in such structures (up to 7.69%), favoring the usage of low-cost MoS_2–carbon hybrid structures as Pt-free counter electrodes in DSSCs.[128]

$MoSe_2$ also plays an essential role in increasing the efficiency of Cu(In,Ga)Se_2 (CIGS) based thin film solar cells with Mo (or possibly ITO—indium tin oxide) as the back electrode.[129,130] CIGS photovoltaic devices are favorable because of their high absorption coefficient reaching 19.9%.[129] It is suggested that $Mo/MoSe_2$/CIGS quasi-ohmic with the interface layer of $MoSe_2$,[129] has an increased conversion efficiency in comparison to Mo (or ITO)/$MoSe_2$/CIGS due to both reduced recombination and ohmic contact resistance, owing to the interface $MoSe_2$ layer.[130]

MoO_3 has been extensively used in organic photovoltaics (OPVs) and organic light emitting diodes (OLEDs).[131] The MoO_3 nano-thin interfacial films are commonly used as hole injection/extraction,[132] and charge generation/recombination layers.[131,133,134] MoO_3/organic interfaces offer effective hole current to electron current conversion. MoO_3 has an electronic structure that is compatible to those of many organic semiconductors, it has low optical absorption in the visible spectrum (bandgap ≈ 3 eV) and a high work function.[131,135] Furthermore, the stability of MoO_3 offers protection for organic coatings from dissolving during further processing.[131,134] Recent comprehensive reviews on the mechanisms and usage of MoO_3 in OPVs are found elsewhere.[131]

5.7. Sensors

2D MT&Ds offer great potential for the development of highly sensitive and low cost sensors. This includes optical, gas, bio, electrochemical and electromechanical sensors. The tunability of the bandgap allows for the fabrication of photodiodes and phototransistors that are engineered to almost any desired wavelengths in the UV, visible and IR regions. FETs based on 2D MoS_2 have been demonstrated as phototransistors.[13,136] Voltage transfer curves and dynamic responses of such phototransistors are presented in **Figure 9**. Single-layer MoS_2 is tuned to the energy bandgap of 1.8 eV, while the bandgap of double- and triple-layered MoS_2 is reduced to 1.65 and 1.35 eV, respectively.

Sensors based on 2D MT&Ds offer great possibilities for developing highly sensitive, semiconductive gas detection systems. Their remarkable sensitivity is based on the fact that the 2D layers are very sensitive to embedded Coloumbic charges. It is well-known that gas and vapor molecules can reduce or oxidize MT&Ds hence, this results in both a change of carrier

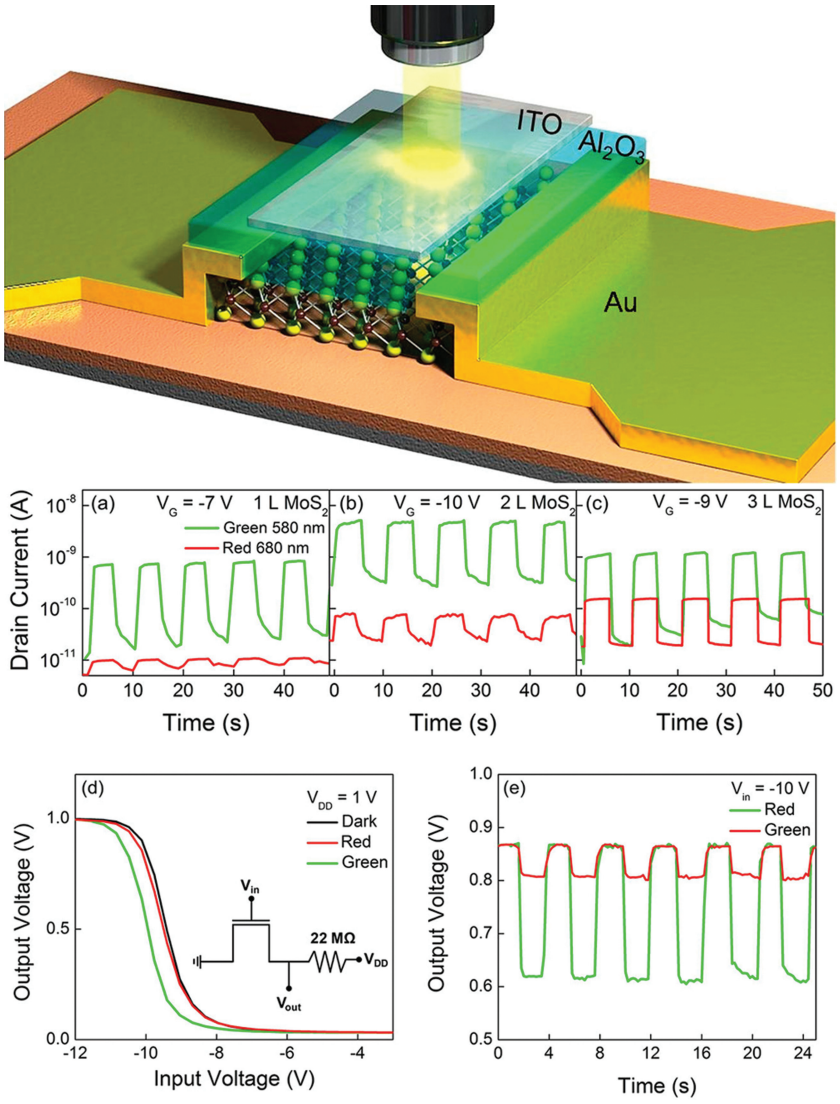

Figure 9. Schematic 3D view of monolayer MoS_2 phototransistor, with thick Al_2O_3 (50 nm) dielectric, and ITO topgate under monochromatic light. Respective photocurrent dynamics of a) mono-, b) bi-, and c) tri-layer MoS_2 transistors under monochromatic red and green lights. d) Dark and photo induced VTC curves of a photo-inverter composed of serially connected resistor and bilayer MoS_2 transistor (see the inset for the circuit). e) Voltage dynamics of the resistive type photo-inverter under monochromatic red and green lights. Reproduced with permission.[13] Copyright 2012, American Chemical Society.

charge mobility (according to Equation (1)) and carrier concentration. These, in turn, change the conductivity of each layer, which can be readily measured. This effect can also be used in the development of sensitive electrochemical transducers. The Born approximation equation also suggests that the 2D films will be extremely sensitive to the materials that are adsorbed onto their surfaces and generate roughness changes. Biomaterials such as proteins, when adsorbed onto the surface of the 2D layers, change both the surface roughness and the permittivity, therefore causing changes in the electronic properties of each layer. Along these lines, it has been shown that 2D MT&D based sensors are highly sensitive to toxic gases and pollutants, as well as various chemical and biological agents.[137,138] Zang et al. have demonstrated the applicability of single and multilayered MoS_2 FETs as room temperature highly sensitive (detection limit of 0.8 ppm) NO gas sensors.[138] More recently, they have also developed flexible gas sensor arrays for detecting NO_2, based on MoS_2 thin film transistors with reduced graphene oxide electrodes.[137] Highly selective chemical vapor sensing properties towards organic compounds have also been reported in monolayered MoS_2.[139] Furthermore, the addition of well-known catalysts such as Pt or Au onto the surface of the 2D layer increases the sensitivity. Electrochemically reduced monolayer MoS_2 nanosheets with good conductivity, superior electron transfer rates and high electrochemical activity have been successfully used for detecting glucose and biomolecules.[140] In addition, they have also demonstrated selectivity towards dopamine in the presence of ascorbic acid and uric acid.

α-MoO_3 has been extensively studied in gas sensing applications, having noticeable surface sensitivity to both reducing

and oxidizing gases at elevated operating temperatures. Its sensing activity originates from chemisorbed gas species and changes in either intercalation or degree of stoichiometry. α-MoO_3 thin films have been demonstrated to be highly sensitive towards various gas species including CO, H_2 NO, NO_2, and NH_3 at the operating temperature range of 200–300 °C.[49,141,142] However, above this temperature range, operation is not viable for sensing applications due to the low sublimation point of MoO_3.[141] Surface acoustic wave (SAW) gas sensors incorporating MoO_3 nano-platelet layers have shown excellent room-temperature sensitivity for methanol detection.[143] It has also been established as a H_2 sensor, as α-MoO_3 shows excellent gasochromic characteristics.[144] In addition, doped and composite α-MoO_3 structures have also been demonstrated to detect H_2S, NO_2, O_3, and volatile organic compounds such as methanol and ethanol.[145]

As described in previous sections, electric field and mechanical stress can also change the electronic structure and vibrational modes of low dimensional MT&Ds. The full incorporation of such properties into the development of sensors and actuators has yet to be fully explored.

5.8. Superconductivity

Low temperature superconductivity in MT&Ds has been studied since the 1970s.[146] The easily tunable band structure and the lamellar layered nature of these crystals have established them as potentially viable for applications in superconductivity. As discussed earlier, layered MDs' band structures can be easily manipulated from semiconductor to metallic by various methods and such a transition at low temperatures was observed to induce superconductivity. In early studies Woolam et al. reported that various alkali metal intercalated MoS_2 compounds exhibit superconductivity at temperatures around 7 K.[146] They suggested that the materials with the largest ionic intercalant diameters and hexagonal crystal structures have the highest critical temperatures and critical fields in comparison to smaller intercalants. Further studies based on potassium (K) and rubidium (Rb) intercalated MoS_2 have also revealed superconducting behaviour at temperatures ranging from 8–12 K.[147,148] This behaviour is attributed to the transfer of electrons from the intercalant to the unfilled *d* band of the MoS_2 structure.[148] More recently, Taniguchi et al. have demonstrated electric field induced superconductivity in MoS_2 structures (at 9.4 K).[149] Additionally, MoO_3 has been adopted as a composite additive in the cuprate superconductor $YBa_2Cu_3O_y$ to enhance its semiconducting temperatures.[150] The possibilities of higher temperature-higher field superconductors via other intercalants in MT&Ds have yet to be explored.

6. Conclusions and Future Outlook

We have presented the fundamentals of lamellar MT&Ds and their properties when they are exfoliated into mono- or multi-layered planes. These materials offer numerous advantages including relative abundance in nature, relative natural stability, a large number of well-investigated synthesis techniques, perfect crystallinity within planar directions, and the possibility of creating crystals with desired stoichiometry. We have demonstrated how their electronic structures such as bandgap can be tuned using a variety of chemical and physical means, including electric, mechanical, and electrochemical forces. When MT&Ds are exfoliated into mono- or limited layers they can restrain the motion of electric charges within the planes, showing strong quantum confinement in the direction normal to the surface of the layers. As such they become extremely sensitive to mechanical, chemical and electrical stimuli in low planar dimensions, which can be used for the development of a variety of transducers. Electronic, optical, thermal, catalytic, electrochromic, magnetic and superconductive properties reported to date have also been summarized. The possible thickness dependence of properties such as bandgap, change in the mobility of electric charges and vibrational modes and their high degree of tunability allow for the creation of functional optical, mechanical, and electronic materials with applications in electronic devices, optoelectronics, nanoelectromechanical (NEMS) systems and sensors. More detailed investigations should be conducted to provide further insights.

We believe that this is just the beginning of a new era for planar MT&Ds. They will certainly play increasingly more important roles in research of semiconductors and possibly become a rival to silicon in certain applications. Their structure is compatible with 2D graphene with the extra advantage that they also provide an intrinsic bandgap, necessary for forming functional FETs and optical devices. It is possible to form composite planar materials with various electronic properties that offer extraordinary superlattice structures with remarkable functionalities.

Perhaps the most promising future applications of low-dimensional MT&Ds are in the electronics industry. To date both MoX_2 and MoO_3 thin layers have shown their potential for the creation of FETs with mobilities comparable (for MoX_2) and almost larger (for sub stoichiometric MoO_3) than those of silicon. It is quite possible to break the current records of electron mobility by one or two orders of magnitudes via dielectric engineering and creating multi-layers of different metal chalcogenides into high electron mobility transistor (HEMT) structures. It is envisaged that by using a layer as the electron injection media and the other layers as the media for mobile charge carriers at low scattering, efficient HEMT structures are possible.

These MT&Ds can provide great solutions for energy storage due to their layered nature that allows for a large number of ions to be intercalated and stored within their lattice. Their planar structure also allows for the fast movement of these ions in and out, which provide facile access and high-energy release rates needed for industrial devices.

The NEMS properties of lamellar and low-dimensional MT&Ds have been less studied. They certainly have the potential to be used in micro/nano mechanical systems for the creation of highly sensitive sensors and low dimensional actuators.

There are many more applications that can be considered and are yet to be investigated. The versatilities of lamellar and low-dimensional planar MT&Ds are extraordinary, which demand intensive and more focused studies in this vibrant and rapidly growing field.

Acknowledgements

S.S. and M.B. acknowledge Australian Post-Doctoral Fellowships from the Australian Research Council through Discovery Projects DP110100262 and DP1092717, respectively. S.S. and K.K.Z. acknowledge the Australian Research Council for equipment funding through the Linkage, Infrastructure, Equipment, and Facilities Grant LE100100215. The work was partially supported by the CSIRO Sensors and Sensor Networks Transformational Capability Platform (SSN TCP) and CSIRO Materials Science and Engineering Division (CMSE).

Received: January 11, 2013
Published online: April 2, 2013

[1] a) M. Xu, T. Liang, M. Shi, H. Chen, *Chem. Rev.* **2013**, DOI: 10.1021/cr300263a; b) Q. H. Wang, K. Kalantar-zadeh, A. Kis, J. N. Coleman, M. S. Strano, *Nat. Nanotechnol.* **2012**, *7*, 699.
[2] S. Balendhran, J. Deng, J. Z. Ou, S. Walia, J. Scott, J. Tang, K. L. Wang, M. R. Field, S. Russo, S. Zhuiykov, M. S. Strano, N. Medhekar, S. Sriram, M. Bhaskaran, K. Kalantar-zadeh, *Adv. Mater.* **2013**, *25*, 109.
[3] K. Kalantar-zadeh, J. S. Tang, M. S. Wang, K. L. Wang, A. Shailos, K. Galatsis, R. Kojima, V. Strong, A. Lech, W. Wlodarski, R. B. Kaner, *Nanoscale* **2009**, *2*, 429.
[4] K. S. Novoselov, D. Jiang, F. Schedin, T. J. Booth, V. V. Khotkevich, S. V. Morozov, A. K. Geim, *Proc. Natl. Acad. Sci. USA* **2005**, *102*, 10451.
[5] B. Radisavljevic, A. Radenovic, J. Brivio, V. Giacometti, A. Kis, *Nat. Nanotechnol.* **2011**, *6*, 147.
[6] A. Kumar, P. K. Ahluwalia, *Eur. Phys. J. B* **2012**, *85*, 186.
[7] K. F. Mak, C. Lee, J. Hone, J. Shan, T. F. Heinz, *Phys. Rev. Lett.* **2010**, *105*, 136805.
[8] A. N. Enyashin, G. Seifert, *Comput. Theor. Chem.* **2012**, *999*, 13.
[9] P. Johari, V. B. Shenoy, *ACS Nano* **2012**, *6*, 5449.
[10] A. Ramasubramaniam, D. Naveh, E. Towe, *Phys. Rev. B* **2011**, *84*, 205325.
[11] X. W. Sha, L. Chen, A. C. Cooper, G. P. Pez, H. S. Cheng, *J. Phys. Chem. C* **2009**, *113*, 11399.
[12] G. Eda, H. Yamaguchi, D. Voiry, T. Fujita, M. Chen, M. Chhowalla, *Nano Lett.* **2011**, *11*, 5111.
[13] H. S. Lee, S. W. Min, Y. G. Chang, M. K. Park, T. Nam, H. Kim, J. H. Kim, S. Ryu, S. Im, *Nano Lett.* **2012**, *12*, 3695.
[14] A. Splendiani, L. Sun, Y. Zhang, T. Li, J. Kim, C.-Y. Chim, G. Galli, F. Wang, *Nano Lett.* **2010**, *10*, 1271.
[15] a) R. Tenne, M. Redlich, *Chem. Soc. Rev.* **2010**, *39*, 1423; b) S. Hu, X. Wang, *J. Am. Chem. Soc.* **2008**, *130*, 8126.
[16] P. F. Carcia, E. M. McCarron, *Thin Solid Films* **1987**, *155*, 53.
[17] D. Di Yao, J. Z. Ou, K. Latham, S. Zhuiykov, A. P. O'Mullane, K. Kalantar-zadeh, *Cryst. Growth Des.* **2012**, *12*, 1865.
[18] D. O. Scanlon, G. W. Watson, D. J. Payne, G. R. Atkinson, R. G. Egdell, D. S. L. Law, *J. Phys. Chem. C* **2010**, *114*, 4636.
[19] H. D. Zheng, J. Z. Ou, M. S. Strano, R. B. Kaner, A. Mitchell, K. Kalantar-zadeh, *Adv. Funct. Mater.* **2011**, *21*, 2175.
[20] T. Boker, R. Severin, A. Muller, C. Janowitz, R. Manzke, D. Voss, P. Kruger, A. Mazur, J. Pollmann, *Phys. Rev. B* **2001**, *64*, 235305.
[21] B. Schonfeld, J. J. Huang, S. C. Moss, *Acta Crystallogr. B* **1983**, *39*, 404.
[22] A. Enyashin, S. Gemming, G. Seifert, *Eur. Phys. J.: Spec. Top.* **2007**, *149*, 103.
[23] J. Z. Ou, J. L. Campbell, D. Yao, W. Wlodarski, K. Kalantar-zadeh, *J. Phys. Chem. C* **2011**, *115*, 10757.
[24] J. W. Rabalais, R. J. Colton, A. M. Guzman, *Chem. Phys. Lett.* **1974**, *29*, 131.
[25] a) T. Itoh, I. Matsubara, W. Shin, N. Izu, M. Nishibori, *Sens. Actuators, B* **2008**, *128*, 512; b) H. Tagaya, K. Ara, J. Kadokawa, M. Karasu, K. Chiba, *J. Mater. Chem.* **1994**, *4*, 551; c) J. Z. Wang, I. Matsubara, N. Murayama, S. Woosuck, N. Izu, *Thin Solid Films* **2006**, *514*, 329.
[26] a) G. E. Buono-Core, G. Cabello, A. H. Klahn, A. Lucero, M. V. Nunez, B. Torrejon, C. Castillo, *Polyhedron* **2010**, *29*, 1551; b) T. H. Fleisch, G. J. Mains, *J. Chem. Phys.* **1982**, *76*, 780; c) O. Merdrignac-Conanec, P. T. Moseley, *Electrochem. Commun.* **1999**, *1*, 51.
[27] T. Ando, A. B. Fowler, F. Stern, *Rev. Mod. Phys.* **1982**, *54*, 437.
[28] F. Stern, W. E. Howard, *Phys. Rev.* **1967**, *163*, 816.
[29] R. E. Prange, T. W. Nee, *Phys. Rev.* **1968**, *168*, 779.
[30] D. Jena, A. Konar, *Phys. Rev. Lett.* **2007**, *98*, 136805.
[31] S. Kim, A. Konar, W. S. Hwang, J. H. Lee, J. Lee, J. Yang, C. Jung, H. Kim, J. B. Yoo, J. Y. Choi, Y. W. Jin, S. Y. Lee, D. Jena, W. Choi, K. Kim, *Nat. Commun.* **2012**, *3*, 1011.
[32] X. K. Hu, Y. T. Qian, Z. T. Song, J. R. Huang, R. Cao, J. Q. Xiao, *Chem. Mater.* **2008**, *20*, 1527.
[33] T. Siciliano, A. Tepore, E. Filippo, G. Micocci, M. Tepore, *Mater. Chem. Phys.* **2009**, *114*, 687.
[34] S. Sugai, T. Ueda, *Phys. Rev. B* **1982**, *26*, 6554.
[35] T. J. Wieting, A. Grisel, F. Lévy, *Physica B+C* **1980**, *99*, 337.
[36] T. J. Wieting, J. L. Verble, *Phys. Rev. B* **1971**, *3*, 4286.
[37] C. Lee, H. Yan, L. E. Brus, T. F. Heinz, J. Hone, S. Ryu, *ACS Nano* **2010**, *4*, 2695.
[38] H. Li, Q. Zhang, C. C. R. Yap, B. K. Tay, T. H. T. Edwin, A. Olivier, D. Baillargeat, *Adv. Funct. Mater.* **2012**, *22*, 1385.
[39] D. J. Late, B. Liu, H. Matte, C. N. R. Rao, V. P. Dravid, *Adv. Funct. Mater.* **2012**, *22*, 1894.
[40] S. Bertolazzi, J. Brivio, A. Kis, *ACS Nano* **2011**, *5*, 9703.
[41] A. Castellanos-Gomez, M. Poot, G. A. Steele, H. S. J. van der Zant, N. Agraït, G. Rubio-Bollinger, *Adv. Mater.* **2012**, *24*, 772.
[42] T. S. Li, *Phys. Rev. B* **2012**, *85*, 235407.
[43] K. A. N. Duerloo, M. T. Ong, E. J. Reed, *J. Phys. Chem. Lett.* **2012**, *3*, 2871.
[44] V. Varshney, S. S. Patnaik, C. Muratore, A. K. Roy, A. A. Voevodin, B. L. Farmer, *Comput. Mater. Sci.* **2010**, *48*, 101.
[45] J. Y. Kim, S. M. Choi, W. S. Seo, W. S. Cho, *Bull. Korean Chem. Soc.* **2010**, *31*, 3225.
[46] Y. D. Ma, Y. Dai, M. Guo, C. W. Niu, J. B. Lu, B. B. Huang, *Phys. Chem. Chem. Phys.* **2011**, *13*, 15546.
[47] a) J. Etzkorn, H. A. Therese, F. Rocker, N. Zink, U. Kolb, W. Tremel, *Adv. Mater.* **2005**, *17*, 2372; b) J. J. Hu, J. S. Zabinski, J. E. Bultman, J. H. Sanders, A. A. Voevodin, *Cryst. Growth Des.* **2008**, *8*, 2603; c) P. A. Parilla, A. C. Dillon, B. A. Parkinson, K. M. Jones, J. Alleman, G. Riker, D. S. Ginley, M. J. Heben, *J. Phys. Chem. B* **2004**, *108*, 6197; d) R. Sivakumar, R. Gopalakrishnan, M. Jayachandran, C. Sanjeeviraja, *Curr. Appl. Phys.* **2007**, *7*, 51.
[48] a) E. I. Altman, T. Droubay, S. A. Chambers, *Thin Solid Films* **2002**, *414*, 205; b) F. S. Ohuchi, B. A. Parkinson, K. Ueno, A. Koma, *J. Appl. Phys.* **1990**, *68*, 2168; c) Y. M. Shi, W. Zhou, A. Y. Lu, W. J. Fang, Y. H. Lee, A. L. Hsu, S. M. Kim, K. K. Kim, H. Y. Yang, L. J. Li, J. C. Idrobo, J. Kong, *Nano Lett.* **2012**, *12*, 2784.
[49] M. B. Rahmani, S. H. Keshmiri, J. Yu, A. Z. Sadek, L. Al-Mashat, A. Moafi, K. Latham, Y. X. Li, W. Wlodarski, K. Kalantar-zadeh, *Sens. Actuators, B* **2010**, *145*, 13.
[50] S. Balendhran, J. Z. Ou, M. Bhaskaran, S. Sriram, S. Ippolito, Z. Vasic, E. Kats, S. Bhargava, S. Zhuiykov, K. Kalantar-zadeh, *Nanoscale* **2012**, *4*, 461.
[51] J. H. Zhan, Z. D. Zhang, X. F. Qian, C. Wang, Y. Xie, Y. T. Qian, *Mater. Res. Bull.* **1999**, *34*, 497.
[52] P. R. Bonneau, R. F. Jarvis, R. B. Kaner, *Nature* **1991**, *349*, 510.
[53] K. A. Gesheva, T. M. Ivanova, G. Bodurov, *Prog. Org. Coat.* **2012**, *74*, 635.

[54] Y. J. Lee, W. T. Nichols, D. G. Kim, Y. Do Kim, *J. Phys. D: Appl. Phys.* **2009**, *42*, 115419.
[55] S. Helveg, J. V. Lauritsen, E. LÃ¦gsgaard, I. Stensgaard, J. K. NÃrskov, B. S. Clausen, H. TopsÃe, F. Besenbacher, *Phys. Rev. Lett.* **2000**, *84*, 951.
[56] Y. Zhan, Z. Liu, S. Najmaei, P. M. Ajayan, J. Lou, *Small* **2012**, *8*, 966.
[57] Y. H. Lee, X. Q. Zhang, W. J. Zhang, M. T. Chang, C. T. Lin, K. D. Chang, Y. C. Yu, J. T. W. Wang, C. S. Chang, L. J. Li, T. W. Lin, *Adv. Mater.* **2012**, *24*, 2320.
[58] Y.-C. Lin, W. Zhang, J.-K. Huang, K.-K. Liu, Y.-H. Lee, C.-T. Liang, C.-W. Chu, L.-J. Li, *Nanoscale* **2012**, *4*, 6637.
[59] M. Diskus, O. Nilsen, H. Fjellvag, *J. Mater. Chem.* **2011**, *21*, 705.
[60] a) A. Guerfi, R. W. Paynter, L. H. Dao, *J. Electrochem. Soc.* **1995**, *142*, 3457; b) R. S. Patil, M. D. Uplane, P. S. Patil, *Appl. Surf. Sci.* **2006**, *252*, 8050.
[61] a) A. Michailovski, G. R. Patzke, *Chem.-Eur. J.* **2006**, *12*, 9122; b) A. Phuruangrat, J. S. Chen, X. W. Lou, O. Yayapao, S. Thongtem, T. Thongtem, *Appl. Phys. A: Mater.* **2012**, *107*, 249; c) C. V. Subba Reddy, E. H. Walker Jr., C. Wen, S.-i. Mho, *J. Power Sources* **2008**, *183*, 330; d) S. Wang, Y. Zhang, X. Ma, W. Wang, X. Li, Z. Zhang, Y. Qian, *Solid State Commun.* **2005**, *136*, 283.
[62] X. Chen, R. Fan, *Chem. Mater.* **2001**, *13*, 802.
[63] Y. Y. Peng, Z. Y. Meng, C. Zhong, J. Lu, W. C. Yu, Y. B. Jia, Y. T. Qian, *Chem. Lett.* **2001**, 772.
[64] a) H. Matte, B. Plowman, R. Datta, C. N. R. Rao, *Dalton Trans.* **2011**, *40*, 10322; b) H. Matte, A. Gomathi, A. K. Manna, D. J. Late, R. Datta, S. K. Pati, C. N. R. Rao, *Angew. Chem. Int. Edit.* **2010**, *49*, 4059.
[65] A. K. Prasad, D. J. Kubinski, P. I. Gouma, *Sens. Actuators, B* **2003**, *93*, 25.
[66] C. Altavilla, M. Sarno, P. Ciambelli, *Chem. Mater.* **2011**, *23*, 3879.
[67] a) W. Ki, X. Y. Huang, J. Li, D. L. Young, Y. Zhang, *J. Mater. Res.* **2007**, *22*, 1390; b) K. K. Liu, W. J. Zhang, Y. H. Lee, Y. C. Lin, M. T. Chang, C. Su, C. S. Chang, H. Li, Y. M. Shi, H. Zhang, C. S. Lai, L. J. Li, *Nano Lett.* **2012**, *12*, 1538.
[68] K. S. Novoselov, A. K. Geim, S. V. Morozov, D. Jiang, Y. Zhang, S. V. Dubonos, I. V. Grigorieva, A. A. Firsov, *Science* **2004**, *306*, 666.
[69] a) M. B. Dines, *J. Chem. Educ.* **1974**, *51*, 221; b) W. M. R. Divigalpitiya, R. F. Frindt, S. R. Morrison, *Science* **1989**, *246*, 369.
[70] a) R. Bissessur, H. Xu, *Mater. Chem. Phys.* **2009**, *117*, 335; b) Z. Ding, L. Viculis, J. Nakawatase, R. B. Kaner, *Adv. Mater.* **2001**, *13*, 797.
[71] Z. Y. Zeng, Z. Y. Yin, X. Huang, H. Li, Q. Y. He, G. Lu, F. Boey, H. Zhang, *Angew. Chem. Int. Ed.* **2011**, *50*, 11093.
[72] R. Bissessur, J. Heising, W. Hirpo, M. Kanatzidis, *Chem. Mater.* **1996**, *8*, 318.
[73] R. J. Smith, P. J. King, M. Lotya, C. Wirtz, U. Khan, S. De, A. O'Neill, G. S. Duesberg, J. C. Grunlan, G. Moriarty, J. Chen, J. Wang, A. I. Minett, V. Nicolosi, J. N. Coleman, *Adv. Mater.* **2011**, *23*, 3944.
[74] a) J. N. Coleman, M. Lotya, A. O'Neill, S. D. Bergin, P. J. King, U. Khan, K. Young, A. Gaucher, S. De, R. J. Smith, I. V. Shvets, S. K. Arora, G. Stanton, H. Y. Kim, K. Lee, G. T. Kim, G. S. Duesberg, T. Hallam, J. J. Boland, J. J. Wang, J. F. Donegan, J. C. Grunlan, G. Moriarty, A. Shmeliov, R. J. Nicholls, J. M. Perkins, E. M. Grieveson, K. Theuwissen, D. W. McComb, P. D. Nellist, V. Nicolosi, *Science* **2011**, *331*, 568; b) G. Cunningham, M. Lotya, C. S. Cucinotta, S. Sanvito, S. D. Bergin, R. Menzel, M. S. P. Shaffer, J. N. Coleman, *ACS Nano* **2012**, *6*, 3468.
[75] Y. G. Yao, Z. Y. Lin, Z. Li, X. J. Song, K. S. Moon, C. P. Wong, *J. Mater. Chem.* **2012**, *22*, 13494.
[76] A. Castellanos-Gomez, M. Barkelid, A. M. Goossens, V. E. Calado, H. S. J. van der Zant, G. A. Steele, *Nano Lett.* **2012**, *12*, 3187.
[77] H. Li, G. Lu, Z. Y. Yin, Q. Y. He, Q. Zhang, H. Zhang, *Small* **2012**, *8*, 682.
[78] I. M. Allam, *J. Mater. Sci.* **1991**, *26*, 3977.
[79] a) T. Onodera, Y. Morita, R. Nagumo, R. Miura, A. Suzuki, H. Tsuboi, N. Hatakeyama, A. Endou, H. Takaba, F. Dassenoy, C. Minfray, L. Joly-Pottuz, M. Kubo, J. M. Martin, A. Miyamoto, *J. Phys. Chem. B* **2010**, *114*, 15832; b) T. Onodera, Y. Morita, A. Suzuki, M. Koyama, H. Tsuboi, N. Hatakeyama, A. Endou, H. Takaba, M. Kubo, F. Dassenoy, C. Minfray, L. Joly-Pottuz, J. M. Martin, A. Miyamoto, *J. Phys. Chem. B* **2009**, *113*, 16526.
[80] S. Kamiya, D. Tsuda, K. Miura, N. Sasaki, *Wear* **2004**, *257*, 1133.
[81] M. Chhowalla, G. A. J. Amaratunga, *Nature* **2000**, *407*, 164.
[82] C. Grossiord, K. Varlot, J. M. Martin, T. Le Mogne, C. Esnouf, K. Inoue, *Tribol. Int.* **1998**, *31*, 737.
[83] E. Bergmann, G. Melet, C. Muller, A. Simonvermot, *Tribol. Int.* **1981**, *14*, 329.
[84] J. M. Martin, C. Donnet, T. Le Mogne, T. Epicier, *Phys. Rev. B* **1993**, *48*, 10583.
[85] a) B. W. Faughnan, R. S. Crandall, *Appl. Phys. Lett.* **1977**, *31*, 834; b) J. N. Yao, B. H. Loo, K. Hashimoto, A. Fujishima, *J. Electroanal. Chem.* **1990**, *290*, 263; c) J. N. Yao, Y. A. Yang, B. H. Loo, *J. Phys. Chem. B* **1998**, *102*, 1856.
[86] J. Z. Ou, S. Balendhran, M. R. Field, D. G. McCulloch, A. S. Zoolfakar, R. A. Rani, S. Zhuiykov, A. P. O'Mullane, K. Kalantar-zadeh, *Nanoscale* **2012**, *4*, 5980.
[87] a) B. Radisavljevic, M. B. Whitwick, A. Kis, *ACS Nano* **2011**, *5*, 9934; b) B. Radisavljevic, M. B. Whitwick, A. Kis, *Appl. Phys. Lett.* **2012**, *101*, 115419; c) H. Wang, L. L. Yu, Y. H. Lee, Y. M. Shi, A. Hsu, M. L. Chin, L. J. Li, M. Dubey, J. Kong, T. Palacios, *Nano Lett.* **2012**, *12*, 4674.
[88] W. Bao, X. Cai, D. Kim, K. Sridhara, M. S. Fuhrer, *Appl. Phys. Lett.* **2013**, *102*, 042104.
[89] S. Das, H.-Y. Chen, A. V. Penumatcha, J. Appenzeller, *Nano Lett.* **2012**, *13*, 100.
[90] S. Larentis, B. Fallahazad, E. Tutuc, *Appl. Phys. Lett.* **2012**, *101*, 223104.
[91] R. Spah, M. Luxsteiner, M. Obergfell, E. Bucher, S. Wagner, *Appl. Phys. Lett.* **1985**, *47*, 871.
[92] J. P. Lu, C. Sun, M. R. Zheng, Y. H. Wang, M. Nripan, J. A. van Kan, S. G. Mhaisalkar, C. H. Sow, *J. Phys. Chem. C* **2012**, *116*, 22015.
[93] a) K. F. Mak, K. L. He, J. Shan, T. F. Heinz, *Nat. Nanotechnol.* **2012**, *7*, 494; b) H. L. Zeng, J. F. Dai, W. Yao, D. Xiao, X. D. Cui, *Nat. Nanotechnol.* **2012**, *7*, 490.
[94] H. Liu, D. W. Su, R. F. Zhou, B. Sun, G. X. Wang, S. Z. Qiao, *Adv. Energy Mater.* **2012**, *2*, 970.
[95] G. Du, Z. Guo, S. Wang, R. Zeng, Z. Chen, H. Liu, *Chem. Commun.* **2010**, *46*, 1106.
[96] H. Hwang, H. Kim, J. Cho, *Nano Lett.* **2011**, *11*, 4826.
[97] K. Chang, W. X. Chen, *J. Mater. Chem.* **2011**, *21*, 17175.
[98] K. Chang, W. X. Chen, L. Ma, H. Li, H. Li, F. H. Huang, Z. D. Xu, Q. B. Zhang, J. Y. Lee, *J. Mater. Chem.* **2011**, *21*, 6251.
[99] X. Zhou, L.-J. Wan, Y.-G. Guo, *Chem. Commun.* **2013**, DOI: 10.1039/c3cc38780a.
[100] a) K. Chang, W. X. Chen, *ACS Nano* **2011**, *5*, 4720; b) K. Chang, W. X. Chen, *Chem. Commun.* **2011**, *47*, 4252.
[101] X. Zhou, L.-J. Wan, Y.-G. Guo, *Nanoscale* **2012**, *4*, 5868.
[102] a) Y. L. Liang, R. J. Feng, S. Q. Yang, H. Ma, J. Liang, J. Chen, *Adv. Mater.* **2011**, *23*, 640; b) S. Q. Yang, D. X. Li, T. R. Zhang, Z. L. Tao, J. Chen, *J. Phys. Chem. C* **2012**, *116*, 1307.
[103] J. Morales, J. Santos, J. L. Tirado, *Solid State Ionics* **1996**, *83*, 57.
[104] L. Campanel, *J. Electrochem. Soc.* **1971**, *118*, 1905.
[105] C. Julien, O. M. Hussain, L. Elfarh, M. Balkanski, *Solid State Ionics* **1992**, *53*, 400.
[106] a) J. W. Bullard III, R. L. Smith, *Solid State Ionics* **2003**, *160*, 335; b) A. M. Hashem, H. Groult, A. Mauger, K. Zaghib, C. M. Julien, *J. Power Sources* **2012**, *219*, 126.
[107] L. Q. Mai, B. Hu, W. Chen, Y. Y. Qi, C. S. Lao, R. S. Yang, Y. Dai, Z. L. Wang, *Adv. Mater.* **2007**, *19*, 3712.

[108] Z. Y. Wang, S. Madhavi, X. W. Lou, *J. Phys. Chem. C* **2012**, *116*, 12508.
[109] a) M. F. Hassan, Z. P. Guo, Z. Chen, H. K. Liu, *J. Power Sources* **2010**, *195*, 2372; b) L. C. Yang, W. L. Guo, Y. Shi, Y. P. Wu, *J. Alloys Compd.* **2010**, *501*, 218.
[110] a) W. Tang, L. L. Liu, Y. S. Zhu, H. Sun, Y. P. Wu, K. Zhu, *Energ. Environ. Sci.* **2012**, *5*, 6909; b) N. Gunawardhana, G.-J Park, N. Dimov, A. K. Thapa, H. Nakamura, H. Wang, T. Ishihara, M. Yoshio, *J. Power Sources* **2011**, *196*, 7886.
[111] a) Z. D. Huang, W. Bensch, L. Kienle, S. Fuentes, G. Alonso, C. Ornelas, *Catal. Lett.* **2008**, *122*, 57; b) B. Yoosuk, J. H. Kim, C. Song, C. Ngamcharussrivichai, P. Prasassarakich, *Catal. Today* **2008**, *130*, 14; c) X. Zong, H. J. Yan, G. P. Wu, G. J. Ma, F. Y. Wen, L. Wang, C. Li, *J. Am. Chem. Soc.* **2008**, *130*, 7176.
[112] B. Hinnemann, P. G. Moses, J. Bonde, K. P. Jorgensen, J. H. Nielsen, S. Horch, I. Chorkendorff, J. K. Norskov, *J. Am. Chem. Soc.* **2005**, *127*, 5308.
[113] T. F. Jaramillo, K. P. Jorgensen, J. Bonde, J. H. Nielsen, S. Horch, I. Chorkendorff, *Science* **2007**, *317*, 100.
[114] P. Raybaud, J. Hafner, G. Kresse, S. Kasztelan, H. Toulhoat, *J. Catal.* **2000**, *189*, 129.
[115] a) J. Chen, S. L. Li, Q. Xu, K. Tanaka, *Chem. Commun.* **2002**, *38*, 1722; b) M. Daage, R. R. Chianelli, *J. Catal.* **1994**, *149*, 414; c) K. H. Hu, X. G. Hu, X. J. Sun, *Appl. Surf. Sci.* **2010**, *256*, 2517.
[116] Y. G. Li, H. L. Wang, L. M. Xie, Y. Y. Liang, G. S. Hong, H. J. Dai, *J. Am. Chem. Soc.* **2011**, *133*, 7296.
[117] H. Bolivar, S. Izquierdo, R. Tremont, C. R. Cabrera, *J. Appl. Electrochem.* **2003**, *33*, 1191.
[118] J. Sonneman, P. Mars, *J. Catal.* **1973**, *31*, 209.
[119] R. Grabowski, B. Grzybowska, K. Samson, J. Sloczynski, J. Stoch, K. Wcislo, *Appl. Catal., A* **1995**, *125*, 129.
[120] T. Waters, R. A. J. O'Hair, A. G. Wedd, *J. Am. Chem. Soc.* **2003**, *125*, 3384.
[121] a) P. Arnoldy, J. A. M. Vandenheijkant, G. D. Debok, J. A. Moulijn, *J. Catal.* **1985**, *92*, 35; b) G. Busca, L. Lietti, G. Ramis, F. Berti, *Appl. Catal., B* **1998**, *18*, 1.
[122] a) H. C. Hu, I. E. Wachs, S. R. Bare, *J. Phys. Chem.* **1995**, *99*, 10897; b) M. M. Mohamed, *Appl. Catal., A* **2004**, *267*, 135; c) S. B. Umbarkar, A. V. Biradar, S. M. Mathew, S. B. Shelke, K. M. Malshe, P. T. Patil, S. P. Dagde, S. P. Niphadkar, M. K. Dongare, *Green Chem.* **2006**, *8*, 488; d) S. B. Umbarkar, T. V. Kotbagi, A. V. Biradar, R. Pasricha, J. Chanale, M. K. Dongare, A. S. Mamede, C. Lancelot, E. Payen, *J. Mol. Catal., A* **2009**, *310*, 150.
[123] X. B. Chen, S. H. Shen, L. J. Guo, S. S. Mao, *Chem. Rev.* **2010**, *110*, 6503.
[124] J. P. Wilcoxon, *J. Phys. Chem. B* **2000**, *104*, 7334.
[125] a) E. Gourmelon, O. Lignier, H. Hadouda, G. Couturier, J. C. Bernede, J. Tedd, J. Pouzet, J. Salardenne, *Sol. Energ. Mater. Sol. Cells* **1997**, *46*, 115; b) V. M. Pathak, K. D. Patel, R. J. Pathak, R. Srivastava, *Sol. Energ. Mater. Sol. Cells* **2002**, *73*, 117.
[126] M. X. Wu, Y. D. Wang, X. Lin, N. S. Yu, L. Wang, L. L. Wang, A. Hagfeldt, T. L. Ma, *Phys. Chem. Chem. Phys.* **2011**, *13*, 19298.
[127] a) J.-Y. Lin, C.-Y. Chan, S.-W. Chou, *Chem. Commun.* **2013**, *49*, 1440; b) C.-J. Liu, S.-Y. Tai, S.-W. Chou, Y.-C. Yu, K.-D. Chang, S. Wang, F. S.-S. Chien, J.-Y. Lin, T.-W. Lin, *J. Mater. Chem.* **2012**, *22*, 21057; c) S.-Y. Tai, C.-J. Liu, S.-W. Chou, F. S.-S. Chien, J.-Y. Lin, T.-W. Lin, *J. Mater. Chem.* **2012**, *22*, 24753.
[128] G. Yue, J. Wu, Y. Xiao, M. Huang, J. Lin, J.-Y. Lin, *J. Mater. Chem. A* **2013**, *1*, 1495.
[129] D. Abou-Ras, G. Kostorz, D. Bremaud, M. Kalin, F. V. Kurdesau, A. N. Tiwari, M. Dobeli, *Thin Solid Films* **2005**, *480*, 433.
[130] a) J. Malmstrom, S. Schleussner, L. Stolt, *Appl. Phys. Lett.* **2004**, *85*, 2634; b) R. Wurz, D. F. Marron, A. Meeder, A. Rumberg, S. M. Babu, T. Schedel-Niedrig, U. Bloeck, P. Schubert-Bischoff, M. C. Lux-Steiner, *Thin Solid Films* **2003**, *431*, 398; c) X. L. Zhu, Z. Zhou, Y. M. Wang, L. Zhang, A. M. Li, F. Q. Huang, *Sol. Energ. Mater. Sol. Cells* **2012**, *101*, 57.
[131] J. Meyer, S. Hamwi, M. Kroger, W. Kowalsky, T. Riedl, A. Kahn, *Adv. Mater.* **2012**, *24*, 5408.
[132] I. Hancox, K. V. Chauhan, P. Sullivan, R. A. Hatton, A. Moshar, C. P. A. Mulcahy, T. S. Jones, *Energ. Environ. Sci.* **2010**, *3*, 107.
[133] a) P. R. Brown, R. R. Lunt, N. Zhao, T. P. Osedach, D. D. Wanger, L. Y. Chang, M. G. Bawendi, V. Bulovic, *Nano Lett.* **2011**, *11*, 2955; b) X. W. Sun, D. W. Zhao, L. Ke, A. K. K. Kyaw, G. Q. Lo, D. L. Kwong, *Appl. Phys. Lett.* **2010**, *97*, 053303.
[134] A. K. K. Kyaw, X. W. Sun, C. Y. Jiang, G. Q. Lo, D. W. Zhao, D. L. Kwong, *Appl. Phys. Lett.* **2008**, *93*, 221107.
[135] D. W. Zhao, X. W. Sun, C. Y. Jiang, A. K. K. Kyaw, G. Q. Lo, D. L. Kwong, *Appl. Phys. Lett.* **2008**, *93*, 083305.
[136] Z. Y. Yin, H. Li, H. Li, L. Jiang, Y. M. Shi, Y. H. Sun, G. Lu, Q. Zhang, X. D. Chen, H. Zhang, *ACS Nano* **2012**, *6*, 74.
[137] Q. Y. He, Z. Y. Zeng, Z. Y. Yin, H. Li, S. X. Wu, X. Huang, H. Zhang, *Small* **2012**, *8*, 2994.
[138] H. Li, Z. Y. Yin, Q. Y. He, H. Li, X. Huang, G. Lu, D. W. H. Fam, A. I. Y. Tok, Q. Zhang, H. Zhang, *Small* **2012**, *8*, 63.
[139] F. K. Perkins, A. L. Friedman, E. Cobas, P. M. Campbell, G. G. Jernigan, B. T. Jonker, *Nano Lett.* **2013**, DOI: 10.1021/nl3043079.
[140] S. X. Wu, Z. Y. Zeng, Q. Y. He, Z. J. Wang, S. J. Wang, Y. P. Du, Z. Y. Yin, X. P. Sun, W. Chen, H. Zhang, *Small* **2012**, *8*, 2264.
[141] E. Comini, L. Yubao, Y. Brando, G. Sberveglieri, *Chem. Phys. Lett.* **2005**, *407*, 368.
[142] M. Ferroni, V. Guidi, G. Martinelli, M. Sacerdoti, P. Nelli, G. Sberveglieri, *Sens. Actuators, B* **1998**, *48*, 285.
[143] M. Penza, A. Z. Sadek, P. Aversa, D. G. McCulloch, W. Wlodarski, K. Kalantar-zadeh, *Sens. Lett.* **2011**, *9*, 920.
[144] a) M. H. Yaacob, J. Yu, K. Latham, K. Kalantar-zadeh, W. Wlodarski, *Sens. Lett.* **2011**, *9*, 16; b) J. Yu, S. J. Ippolito, M. Shafiei, D. Dhawan, W. Wlodarski, K. Kalantar-zadeh, *Appl. Phys. Lett.* **2009**, *94*, 013504.
[145] a) Y. J. Chen, F. N. Meng, C. Ma, Z. W. Yang, C. L. Zhu, Q. Y. Ouyang, P. Gao, J. Q. Li, C. W. Sun, *J. Mater. Chem.* **2012**, *22*, 12900; b) A. Gurlo, N. Barsan, M. Ivanovskaya, U. Weimar, W. Gopel, *Sens. Actuators, B* **1998**, *47*, 92; c) K. Hosono, I. Matsubara, N. Murayama, S. Woosuck, N. Izu, *Chem. Mater.* **2005**, *17*, 349; d) T. S. Wang, Q. S. Wang, C. L. Zhu, Q. Y. Ouyang, L. H. Qi, C. Y. Li, G. Xiao, P. Gao, Y. J. Chen, *Sens. Actuators, B* **2012**, *171*, 256; e) H. L. Yu, L. Li, X. M. Gao, Y. Zhang, F. N. Meng, T. S. Wang, G. Xiao, Y. J. Chen, C. L. Zhu, *Sens. Actuators, B* **2012**, *171*, 679.
[146] J. A. Woollam, R. B. Somoano, *Mater. Sci. Eng.* **1977**, *31*, 289.
[147] S. Bandow, Y. Maruyama, X. X. Bi, R. Ochoa, J. M. Holden, W. T. Lee, P. C. Eklund, *Mater. Sci. Eng., A* **1995**, *204*, 222.
[148] T. K. Gupta, *Phys. Rev. B* **1991**, *43*, 5276.
[149] K. Taniguchi, A. Matsumoto, H. Shimotani, H. Takagi, *Appl. Phys. Lett.* **2012**, *101*, 042603.
[150] a) T. Suzuki, T. Yamazaki, A. Koukitu, M. Maeda, H. Seki, K. Takahashi, *J. Mater. Sci. Lett.* **1988**, *7*, 926; b) M. S. Wu, T. T. Fang, *J. Am. Ceram. Soc.* **1995**, *78*, 1111.
[151] L. H. Brixner, *J. Inorg. Nucl. Chem.* **1962**, *24*, 257.